Marine Micropaleontology 175 (2022) 102134

Contents lists available at ScienceDirect

Marine Micropaleontology

journal homepage: www.elsevier.com/locate/marmicro

Research paper

The Valanginian Weissert Event on the south Tethyan margin: A dynamic paleoceanographic evolution based on the study of calcareous nannofossils

M. Shmeit [a,b,*], F. Giraud [a], E. Jaillard [a], S. Reboulet [c], M. Masrour [d], J.E. Spangenberg [e], A. El-Samrani [b]

[a] Univ. Grenoble Alpes, Univ. Savoie Mont Blanc, CNRS, IRD, Univ. Gustave Eiffel, ISTerre, 38000 Grenoble, France
[b] Lebanese University, Doctoral School of Science and Technology, Laboratory of Geosciences Georesources and Environment L2GE, EDST/PRASE, Beirut, Lebanon
[c] Univ Lyon, UCBL, ENSL, UJM, CNRS, LGL-TPE, F-69622 Villeurbanne, France
[d] Université Ibn Zohr, Faculté des Sciences, Département de Géologie, BP 8106, Cité Dakhla, Agadir, Morocco
[e] University of Lausanne, Institute of Earth Surface Dynamics (IDYST), CH-1015 Lausanne, Switzerland

ARTICLE INFO

Keywords:
Carbon isotope excursion
Central Moroccan margin
Biostratigraphy
Sedimentary evolution
Surface-water fertility

ABSTRACT

Paleoceanographic conditions across the Valanginian Weissert oceanic anoxic event were reconstructed for the first time on the central Moroccan margin from a quantitative-based calcareous nannofossil study. Two onshore successions in the Essaouira-Agadir Basin and one offshore from DSDP Hole 416A were studied, providing a proximal-distal transect on the central Moroccan margin. The paleoceanographic conditions were reconstructed in an accurate chronostratigraphic framework. The sedimentary evolution of the Essaouira-Agadir Basin shows that sea-level variations controlled the paleogeographic context, clastic input, and nutrient availability. A thick photic zone and mesotrophic conditions favored the development of a diverse nannofossil community before the Weissert Event in the early Valanginian. In all studied successions, a collapse of the nannofossil community was recorded during the onset of the Weissert Event at the early-late Valanginian transition, and was caused by a major sea-level fall. The nannofossil community gradually recovered and reached its highest nannofossil production associated with high surface-water fertility during the Weissert Event in the late Valanginian. This eutrophication is coeval with the high and stable $\delta^{13}C_{carb}$ values of the carbon-isotope positive shift. After the Weissert Event, surface-water fertility and nannofossil production decreased but remained higher than during the early Valanginian. Additionally, the nannoconid decline started in the early Valanginian and was linked to a low sea-level. Their recovery in the early late Valanginian occurred during conditions of high sea-level and of high surface-water fertility. The central Moroccan margin is integrated into a global paleoceanographic reconstruction.

1. Introduction

The Valanginian stage (137.7–132.6 Ma; Gale et al., 2020) records the first positive carbon-isotope excursion (CIE) of the Early Cretaceous (Lini et al., 1992; Weissert and Erba, 2004), termed the Weissert oceanic anoxic event or the Weissert Event (Erba et al., 2004; Kujau et al., 2012). The amplitude of the CIE ranges between 1.5 and 2‰ in bulk marine carbonate rock and 1.5–3‰ in marine organic matter (Lini et al., 1992; Hennig et al., 1999; McArthur et al., 2007; Charbonnier et al., 2013). In addition, the positive CIE was recognized in terrestrial fossil plants with a magnitude of ~4‰, implying a perturbation of both the oceanic and atmospheric Earth systems (Gröcke et al., 2005; Nunn et al., 2010). Martinez et al. (2015) identified three phases for the CIE, a first phase of rapid $\delta^{13}C_{carb}$ increase with a duration of 0.60 myr, a second phase of stable $\delta^{13}C_{carb}$ values lasting 1.48 myr, and a final phase of smooth decrease in $\delta^{13}C_{carb}$ values lasting 3.77 myr and extending to the early-late Hauterivian boundary. The onset of the positive CIE was observed just below the early-late Valanginian boundary (Duchamp-Alphonse et al., 2007; McArthur et al., 2007; Gréselle et al., 2011; Martinez et al., 2015). In the Tethyan Realm, the positive CIE was dated from the late NK3A calcareous nannofossil Subzone and extends to the NC4A calcareous nannofossil Subzone in some localities (Lini et al., 1992; Sprovieri et al., 2006; Duchamp-Alphonse et al., 2007; Bornemann and Mutterlose, 2008; Charbonnier et al., 2013; Aguado et al., 2018). Calibrated

* Corresponding author at: Biogéosciences, UMR 6282 CNRS, Université Bourgogne Franche-Comté, 6 Bvd Gabriel, 21000 Dijon, France.
E-mail address: majd.homaidan-shmeit@u-bourgogne.fr (M. Shmeit).

https://doi.org/10.1016/j.marmicro.2022.102134
Received 5 July 2021; Received in revised form 17 May 2022; Accepted 29 May 2022
Available online 2 June 2022

with ammonite biostratigraphy, the onset of the positive CIE was identified in the lower part of the *Karakaschiceras inostranzewi* Standard Zone (uppermost early Valanginian) and the highest values occur during the *Saynoceras verrucosum* Standard Zone (lowermost late Valanginian; McArthur et al., 2007; Gréselle et al., 2011; Martinez et al., 2015; Aguado et al., 2018). The aforementioned zones follow the standard ammonite zonation that is suitable for the Mediterranean Province of the Mediterranean-Caucasian Subrealm (Tethyan Realm; Reboulet et al., 2018). In addition to the Tethyan Realm, records of the positive CIE extend to a wide range of geographic locations that include the Atlantic Ocean (Brenneke, 1978; Cotillon and Rio, 1984), the northwestern Pacific Ocean (Bartolini, 2003), the Boreal Realm (Price and Mutterlose, 2004; Meissner et al., 2015; Morales et al., 2015), and the southern Hemisphere (Aguirre-Urreta et al., 2008; Gómez-Dacal et al., 2018).

The positive CIE has been associated with a global increase in marine surface-water primary productivity (Erba et al., 2004). During the Valanginian, calcareous nannofossils and dinoflagellates were the major marine planktonic primary producers (Bown et al., 2004). Several studies on calcareous nannofossil assemblages have shown enhanced surface-water trophic conditions occurring before and during the Weissert Event, inferred from increasing abundances of high-fertility taxa such as *Biscutum*, *Discorhabdus*, *Diazomatolithus*, and small *Zeugrhabdotus* spp. (Tethyan Realm: Bersezio et al., 2002; Erba and Tremolada, 2004; Duchamp-Alphonse et al., 2007; Mattioli et al., 2014; Atlantic Ocean: Bornemann and Mutterlose, 2008; Kessels et al., 2006; Pacific Ocean: Lozar and Tremolada, 2003; and Boreal Realm: Williams and Bralower, 1995; Melinte and Mutterlose, 2001; Kessels et al., 2006). Nevertheless, paleoceanographic reconstructions based on calcareous nannofossils from the south Tethyan margin have not been documented yet, such that it needs to be further investigated. The causes of the increase in marine primary productivity differ in coastal and distal pelagic settings. Eutrophication in the coastal settings is hypothesized to have been caused by a greenhouse climate, intensification of the hydrological cycle, and consequently higher weathering rates and detrital input (Lini et al., 1992). Climate reconstructions demonstrated intensified hydrolyzing conditions culminating around the early-late Valanginian transition observed from clay mineral distributions (Duchamp-Alphonse et al., 2011; Charbonnier et al., 2020) and spore-pollen ratios (Kujau et al., 2013). Eutrophication in pelagic settings could be explained by the introduction of limiting bio-metals from hydrothermal vents during the break-up of Gondwana (Lini et al., 1992; Weissert et al., 1998; Erba et al., 2004). Sea-level changes might have also influenced the fertilization of the ocean. (1) Enhanced continental runoff increases nutrient fluxes to the proximal parts of the ocean (gradual fertilization) during low sea level. (2) An increase in nutrients within the outer shelf realm may be linked to upwelling (sharp fertilization) during high sea level. In the late Valanginian, a global sea-level rise was documented after an all-time minimum of the Early Cretaceous occurred in the mid-Valanginian (Haq, 2014). The different hypotheses that could cause the fertilization of the ocean need to be tested for the Weissert positive CIE. A biocalcification crisis in both platform and pelagic settings has been inferred from carbonate platform drowning around the early-late Valanginian (Weissert et al., 1998; Wortmann and Weissert, 2000; Föllmi et al., 2006), and a nannoconid decline predating the positive CIE has been identified (Channell et al., 1993; Bersezio et al., 2002; Erba and Tremolada, 2004; Gréselle et al., 2011; Barbarin et al., 2012).

This study aims to reconstruct the paleoceanographic conditions around the Weissert Event on the central Moroccan margin, which was located on the south Tethyan margin during the Cretaceous. Calcareous nannofossil abundances and accumulation rates together with their assemblages were used to quantify changes in surface-water nannofossil production and fertility conditions. Nannofossil samples were collected from three geological successions located on a proximal-distal transect: two onshore sections (Zalidou and Aït Hamouch belonging to the Essaouira-Agadir Basin, EAB) and an offshore DSDP Hole 416A (east Atlantic Ocean). The paleogeographic context of the onshore sections was defined from a sedimentological analysis done at the scale of the EAB. The time framework was based on ammonite (only for the onshore sections) and calcareous nannofossil biostratigraphy, and carbon-isotope stratigraphy. The transect allowed to better constrain the variations of continental nutrient flux, upwellings that were present on the NW African margin during the Early Cretaceous due to active trade winds considering atmospheric circulation models from Price et al. (1995) and Poulsen et al. (1998), and calcareous nannofossil production.

2. Geological setting

The Essaouira-Agadir Basin (EAB) is located in southwest Morocco and corresponds to the westernmost part of the High Atlas fold belt, bounded by 9°55′ to 9°20′ W and 30°30′ to 31°05′ N. The basin is bordered to the north by the Jebilet Massif and Doukkala Plateau (Paleozoic basements), to the south by the plain of Souss (Neogene basin), and to the east by the High Atlas (Fig. 1). The EAB presently constitutes part of the Atlantic passive margin which is considered one of the oldest existing passive margins (Stets and Wurster, 1982; Sahabi et al., 2004). The EAB extends offshore until the western limit of the continental margin (Frizon de Lamotte et al., 2008). During the Cretaceous, the central Moroccan margin which includes the EAB occupied a paleogeographic location on the south Tethyan margin, between paleolatitudes ~15°N and ~ 22°N (Fig. 2). Until the opening of the South Atlantic (Valanginian) and its connection with the Central Atlantic (early Albian), the Tethys Ocean included what is presently the Central Atlantic. Therefore, the geological evolution of the Atlantic-Tethyan passive margin controlled the development of the EAB (Ellouz et al., 2003). Two sections in the EAB, namely Zalidou and Aït Hamouch, were selected for the study of calcareous nannofossils. The Zalidou section is located 45 km north of Agadir (30°54′23”N; 9°39′48”W; Fig. 1B), whereas the Aït Hamouch section is located ~25 km NNW of Agadir (30°36′54”N; 9°42′14”W). The Aït Hamouch section is composed of two adjacent sections, only 0.6 km apart from each other. The primary section, denoted “AH”, was not accessible in its middle part (between 32 and 42 m). Accordingly, the nearby “ATH” section was studied and correlated using ammonite biostratigraphy and sedimentological discontinuities. Moreover, calcareous nannofossils were studied in the offshore succession DSDP Leg 50 Hole 416A (Fig. 1A). Additional sections were used in this paper to improve the precision of the ammonite biostratigraphy and the sedimentological framework (Fig. 1B), although these sections will not be discussed in detail herein as this is beyond the scope of this paper.

2.1. Ammonite zonal framework for the late Berriasian-early Hauterivian interval of the EAB

The systematic revision and identification of ammonites sampled at Zalidou and Aït Hamouch sections are being prepared as a separate paper and were part of a chapter in Shmeit's PhD thesis (2021), in which paleontological comments and ranges of ammonite taxa are provided. The standard ammonite zonation for the Mediterranean Province (Tethyan Realm, Reboulet et al., 2018) is applied here. Only two regional units are added, namely *Neocomites subtenuis* and *Busnardoites campylotoxus* local subzones, to make more accessible the comparisons with previous works made in this Moroccan area by Wippich (2001, 2003) and Ettachfini (2004). The ammonite (sub-)zones are interval (sub-)zones defined by the first appearance datum (FAD) of two successive ammonite-indices. Hereafter will be used the following abbreviations: standard zone = StZ, standard subzone = StSz, and local subzone = LSz.

The base of the *Thurmanniceras pertransiens* StZ, and therefore the lower boundary of the Valanginian, is placed by the FAD of the index-species (Kenjo et al., 2021). As it is relatively rare at Zalidou and Aït Hamouch, the base of the zone can be placed at the first records of

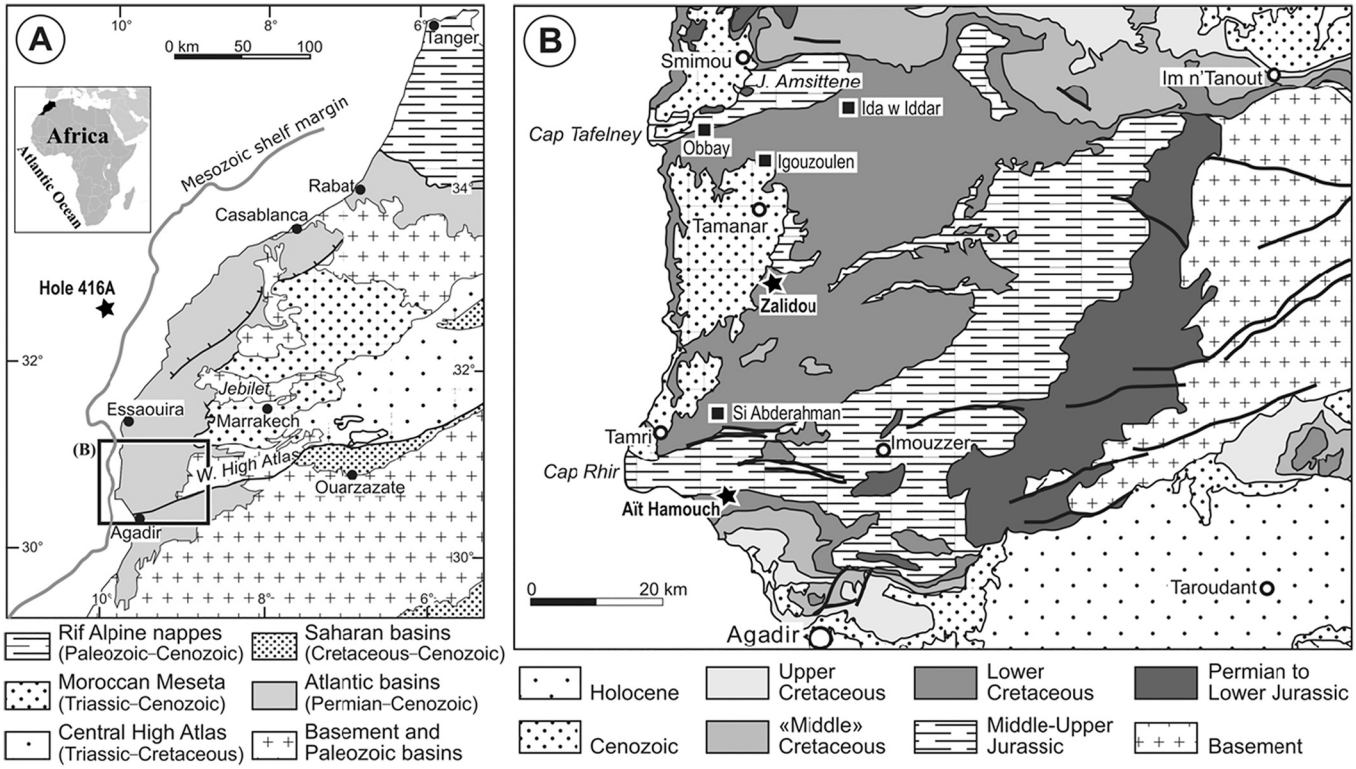

Fig. 1. Location of the study area in SW Morocco, modified from Ouajhain et al. (2009). (A) Location of the central Moroccan margin including the Essaouira-Agadir Basin and the DSDP Hole 416A (not to scale). Approximate location of the Mesozoic shelf margin from Tari and Jabour (2013). (B) Geological sketch including the location of the sections used in this study (square shape). The successions studied for their calcareous nannofossil assemblages (Zalidou, Aït Hamouch, and Hole 416A) are identified in "bold" font and by a "star" sign.

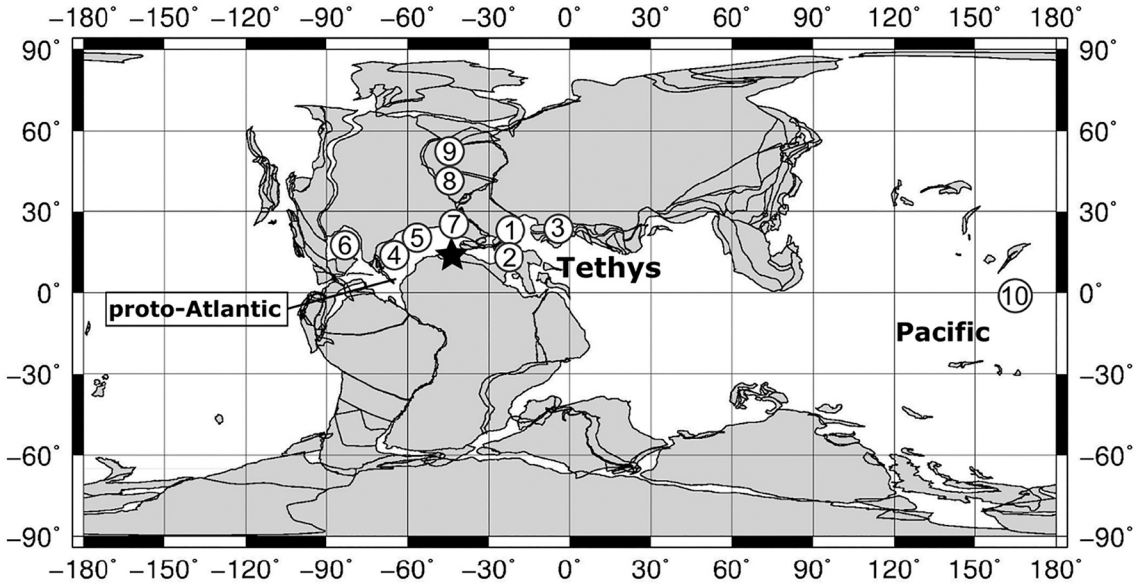

Fig. 2. Paleogeographic map of the Valanginian (136 Ma) showing the location of the central Moroccan margin (star shape). The "white circles" correspond to the location of basins/successions where calcareous nannofossils of the Weissert Event were investigated: Tethyan Realm, (1) Vocontian Basin (France) (Duchamp-Alphonse et al., 2007, 2014; Gréselle et al., 2011; Barbarin et al., 2012; Mattioli et al., 2014), (2) Lombardy Basin (Italy) (Bersezio et al., 2002; Erba and Tremolada, 2004), and (3) Moesian Platform (south and east Carpathians-Romania) (Melinte and Mutterlose, 2001); western and central Atlantic, (4) DSDP 534A (Blake Bahama basin, NE Florida) and (5) DSDP 603B (east Florida) (Bornemann and Mutterlose, 2008), and (6) DSDP 535 (SE Gulf of Mexico) (Kessels et al., 2006); Boreal Realm, (7) ODP 638 (NW Iberian Peninsula) (Kessels et al., 2006), (8) BGS 81/43 (southern North Sea Basin, east England) (Williams and Bralower, 1995; Kessels et al., 2006), and (9) east Greenland Basin (NE Greenland) (Pauly et al., 2012); western Pacific, (10) ODP 1149B (Nadezhda Basin) (Lozar and Tremolada, 2003). Construction from http://www.odsn.de (made from the datafiles of Hay et al. (1999)).

Neocomites premolicus (Ettachfini, 2004; Reboulet et al., 2018). Due to the rarity of the index-species, the base of the *N. neocomiensiformis* StZ is identified at Zalidou and Aït Hamouch sections by the first occurrence (FO) of *Neocomites subtenuis*, as its appearance is contemporaneous with that of *N. neocomiensiformis* in SE Spain (Company and Tavera, 2015). Above the *N. subtenuis* LSz, the upper part of the *N. neocomiensiformis* StZ is characterized by the *Busnardoites campylotoxus* LSz, for which the base is placed at the FO of its relatively abundant index-species at Zalidou and Aït Hamouch. The base of the *Karakaschiceras inostranzewi* StZ is placed at the FO of its index species. In both sections, *Saynoceras verrucosum*, index species of the *S. verrucosum* StZ, was not found. Other ammonite markers of the basal part of this zone, such as *Valanginites ventrotuberculatus*, were also not observed. Consequently, at Zalidou, the base of the *S. verrucosum* StZ, and so the base of the late Valanginian, are placed at the FO of *Karakaschiceras pronecostatum* that is the index-species of the second subzone of the *S. verrucosum* StZ. At Aït Hamouch, very few specimens of some taxa that could be restricted to the *S. verrucosum* StZ are recorded in a single layer (AH89) with the FO of *Neocomites peregrinus* allowing the identification of the base of the *N. peregrinus* StZ. Thus, the ammonite assemblage could be interpreted as a result of a condensed lithology. In this layer, there are also few doubtful specimens of *K. inostranzewi?*; their preservation could indicate that they have been reworked. At Zalidou, *N. peregrinus* was also observed allowing the placement of the base of the zone. In this section, the *Olcostephanus nicklesi* StSz is identified by the occurrence of the genus *Himantoceras* (see Reboulet, 1996). The *O. nicklesi* StSz is not recognized at Aït Hamouch. The base of the *Criosarasinella furcillata* StZ and that of the *Teschenicerasc callidiscum* StSz are identified in both sections. The base of the *Acanthodiscus radiatus* StZ, and thus the base of the Hauterivian (see Mutterlose et al., 2020), are placed at the FO of *Breistrofferella castellanensis* and that of *Acanthodiscus radiatus* at Zalidou and Aït Hamouch, respectively.

2.2. DSDP Hole 416A

DSDP Leg 50 Hole 416A was drilled ~180 km NW of Essaouira (32°50′10.7"N; 10°48′03.6"W) at a water depth of 4201 m in the eastern Atlantic (Fig. Supp. 1). The Berriasian to Hauterivian sediments consist of a turbidite succession deposited in a lowermost continental rise environment (Lancelot et al., 1980). The Valanginian interval was identified onboard from cores 48 to 14, between −1540 and −1222 meters below seafloor (mbsf) (Čepek and Gartner, 1980; Sliter, 1980). The detailed lithology of Hole 416A was described by Lancelot et al. (1980). Briefly, the Berriasian and early Valanginian were assigned to lithological unit VII (from −1624 to −1430 mbsf, cores 57 to 37), characterized by alternating siliciclastic and carbonate turbidites. The lithology displays quartz-rich siltstone and mudstone cycles alternating with hard micritic and calpionellid-rich limestones. A prominent change in lithology above −1430 mbsf characterizes the shift to the overlying lithological unit VI (from to −1430 to −880 mbsf, cores 36 to 7). This change is identified by an abrupt decrease in carbonate deposition and a subsequent increase in terrigenous input, with siliciclastic terrigenous turbidites replacing the calcareous turbidites. The lithology change was regarded as a classical example of the mid-Valanginian platform drowning (Schlager, 1980). Lithological unit VI spans the rest of the Valanginian and builds up to the Hauterivian (Lancelot et al., 1980; Schlager, 1980). The lithology shows graded calcareous and siliciclastic cycles, from siltstone or fine sandstone to mudstone.

3. Materials and methods

The onshore successions (Zalidou and Aït Hamouch) span the late Berriasian to early Hauterivian covering the entire Valanginian. The offshore DSDP Leg 50 Hole 416A spans the Valanginian stage (Čepek and Gartner, 1980). Samples for calcareous nannofossils, calcium carbonate content, and carbon-isotope analyses were collected from different lithologies (except sandstones). The sampling interval was on average 0.3 m in Zalidou, 0.5 m in Aït Hamouch, and 5 m in Hole 416A. Both macrofossils and nannofossil smear slides are curated at the Collections de Géologie de l'Observatoire des Sciences de l'Univers de Grenoble (OSUG), with an appropriate UJF-ID number. "OSUG-COLLECTIONS" is a database of rocks, minerals, and fossils (https://web.collections.osug.fr, OSUG, UGA; doi:https://doi.org/10.5072/OSUG-COLLECTIONS.all).

3.1. Sedimentological analysis

Sedimentological analysis was based on sections located in the southern and central parts of the EAB (Fig. 1B). Observations were made both in the field and under the microscope. All sedimentary features (lithology, peculiar surfaces, sedimentary figures, faunal content, and bioturbation) were observed and recorded in the field. Limestone beds, mainly in the lower Valanginian series, were also sampled for microfacies analysis. We used the classification defined by Dunham (1962).

3.2. Calcareous nannofossils

Biostratigraphic and paleoenvironmental analyses of the Zalidou and Aït Hamouch sections were based on 85 and 54 samples (Supplementary Table), respectively, from calcareous claystone to limestone. For Hole 416A, 44 samples were investigated.

Smear slides were prepared using a random settling technique developed by Beaufort et al. (2014) and modified by Menini et al. (2019). Only 17 samples from the Aït Hamouch "AH section" were prepared using the random settling technique of Geisen et al. (1999) (see Supplementary Table). Both techniques allow the determination of the nannofossil absolute abundance (nannofossils/gram of rock) using the equations presented in the Supplementary Table. A comparison between both techniques for absolute abundance quantification has not been done yet. Studies comparing other slide preparation techniques have shown that nannofossil proportions can be reliably determined regardless of the technique (Bordiga et al., 2015; Lupi et al., 2016).

Nannofossils were observed using a polarizing light microscope (Leica "DM2500 P") at 1000× magnification. Five hundred specimens per slide, both coccoliths and nannoliths, were generally counted in a variable number of fields of view (a mean of 52 for Zalidou, 80 for Aït Hamouch, and 39 for DSDP Hole 416A). All nannofossils with at least more than half of the specimen preserved were counted. In few samples (4 from Zalidou and 3 from Aït Hamouch), characterized by low abundance of nannofossils (approx. 1–2 specimens/4 fields of view), ~350–400 specimens were counted (Supplementary Table). In addition, two longitudinal random transverses (200 fields of view per transverse) were scanned after each counting for rare species that could be of biostratigraphic importance. To improve the biostratigraphic schemes whenever needed, ~8–12 random longitudinal transverses on uncounted samples were also scanned (5 from Zalidou, 1 from Aït Hamouch, and 11 from Hole 416A).

The taxonomic frameworks of Perch-Nielsen (1985), Bown and Young (1997), and Nannotax3 (Young et al., 2017) were followed. For nannoconids, the work of Deres and Achéritéguy (1980) was followed. The calcareous nannofossil zonation applied to the investigated sections were the NC and NK zones of Bralower (1987) and Bralower et al. (1989, 1995), modified from Roth (1978). This zonation scheme was selected because of its applicability to low-latitude Tethyan continental margins and Atlantic oceanic settings (Bralower et al., 1995; Bown, 2005; Bornemann and Mutterlose, 2008). The biostratigraphic scheme (CC zones and subzones) of Sissingh (1977), modified by Perch-Nielsen (1979, 1985) and Applegate and Bergen (1988), was also applied to the studied sections because it allows subdividing the early Valanginian. This zonal scheme uses taxa with cosmopolitan distribution and Tethyan affinities, and it relies on the first occurrence (FO) of *Eiffelithus* taxa (*E. windii* and *E. striatus*) for subzone divisions during the Valanginian stage.

Nannofossil preservation was evaluated following the classes defined by Roth and Thierstein (1972) and modified by Roth (1983). Nannofossil absolute abundances are controlled by the nannoplankton biomass, preservation, and sedimentation rate. Nannofossil accumulation rates (nannofossils/m^2/yr) were calculated to cancel the sedimentation rate effect (see formula in Supplementary Table). The duration of the different phases of the positive CIE from Martinez et al. (2015) were used to determine the sedimentation rates in the studied sections. These authors provided an improved age model for the Valanginian-Hauterivian boundary using astrochronology, and acquired absolute age durations for the different phases of the positive CIE. The $\delta^{13}C_{carb}$ values and the ammonite zonation of the onshore sections (Zalidou and Aït Hamouch) were correlated with those of Martinez et al. (2015).

For each nannofossil taxon (or group of combined taxa) the absolute abundance (AA), the relative abundance (RA), and the accumulation rate (AR, only for the Zalidou and Aït Hamouch sections) were calculated. In addition, the nannofossil total absolute abundance (NTAA) and the nannofossil total accumulation rate (NTAR, for Zalidou and Aït Hamouch sections) were calculated, corresponding to the entire nannofossil assemblage. To consider the inherent counting uncertainty, binomial proportion confidence intervals for relative abundances were computed based on the 'exact' Clopper–Pearson method using the PAST software (Hammer et al., 2001; Suchéras-Marx et al., 2019). Additionally, diversity indices were calculated. *Nannoconus* spp. were excluded from the calculation of sample diversity indices, absolute/relative abundances, and accumulation rates of other taxa because of their uncertain biological affinity (Aubry et al., 2005). The counting and the different calculation formulae are given in the Supplementary Table.

3.3. Calcimetry and carbon isotopes

The calcium carbonate content was measured on 117 and 56 bulk rock samples from Zalidou and Aït Hamouch sections, respectively (Supplementary Table). For Aït Hamouch, analyses were done on samples from the "AH" section. Additionally, 88 samples from DSDP Hole 416A were measured (Supplementary Table). The $CaCO_3$ content was determined using the carbonate bomb technique (Müller and Gastner, 1971). For the calculation of the calcium carbonate percentage, see Appendix A in Peybernes et al. (2013).

Carbon stable isotope analysis was performed on the same samples as for the calcium carbonate content at the stable isotope laboratories of the Institute of Earth Surface Dynamics of the University of Lausanne, using a Thermo Fisher Scientific Gas Bench II carbonate preparation device connected to a Delta Plus XL isotope ratio mass spectrometer. The CO_2 extraction was done at 70 °C. The carbon stable isotope ratios were reported in the delta (δ) notation as the per mil (‰) relative to the Vienna Pee Dee belemnite standard (VPDB), where $\delta = (R_{sample} - R_{standard})/R_{standard}$ and $R = {}^{13}C/{}^{12}C$. The $\delta^{13}C_{carb}$ values were standardized relative to the international VPDB scale by calibration of the reference gases and working standards with international reference materials NBS 18 (carbonatite, $\delta^{13}C = -5.01‰$) and NBS 19 (limestone, $\delta^{13}C = +1.95‰$). Analytical uncertainty (1 sigma), monitored by replicate analyses of the international calcite standard NBS 19 and the laboratory standard Carrara Marble ($\delta^{13}C = +2.05‰$) was not greater than ±0.05‰ for $\delta^{13}C$.

4. Results

4.1. Summary of the Valanginian sedimentary evolution

Geological sections indicated in "bold" font hereafter, correspond to sections that have been investigated for calcareous nannofossils in the present study. Detailed analysis allowed the identification of several sequences. Three main stages can be recognized in the Valanginian sedimentary evolution of the EAB.

1. The top of the Berriasian carbonate shelf is marked by a karstified surface in the northern sections. The overlying lower Valanginian succession (8–15 m) is dominated by marlstone and thin limestone beds (Fig. 3). It shows a thinning-upward, then thickening-upward trend. In the thinning-upward lower part, ammonites, belemnites, plicatulids, and brachiopods dominate. They are also associated with ostreids, *Trichites* sp., pectinids, and with sea-urchins at the base (Fig. 3). Microfacies show mudstone to wackestone textures containing mainly echinoids, bivalves, and agglutinated foraminifers. The fauna indicates an outer shelf depositional environment that represents the maximum depositional depth for the early Valanginian period. In the upper part of the lower Valanginian succession, limestone beds are more abundant and sandstone beds appear in the south (**Aït Hamouch**). The macrofauna is composed of ammonites, belemnites, brachiopods, oysters, and plicatulids, with subordinate regular and irregular sea-urchins, crinoids, serpulids, and locally corals and bone fragments (Fig. 3). Compared with the lower part, this assemblage indicates a shallower depositional depth. Microfacies analysis reveals wackestone textures containing agglutinated foraminifers, brachiopods, echinoids, and benthic foraminifers. Several discontinuities (erosion, karsted surfaces) indicate the existence of three or four depositional sequences, and support a marked shallowing-upward trend that culminated in the late early Valanginian. The Obbay section exhibits a very reduced lower Valanginian succession (3 m), mainly made of limestone beds alternating with thin marlstone interbeds (Fig. 3). Limestones show a wackestone texture containing abundant phosphate-rich glauconitic oolites and are frequently capped by iron-rich hardgrounds. The causes of condensation of this series are discussed in Section 5.1.
2. The lower part of the upper Valanginian series (5–15 m) is mainly made of marlstone, thin limestone beds, sandy marlstone, and sandy limestone. The sandy beds are more abundant to the north and east (Fig. 3). The succession shows a thinning-upward trend, locally overlain by a thickening-upward series, interrupted by a major erosion period (D7) that removed one depositional sequence in many sections (Fig. 3). It contains an outer shelf to hemipelagic macrofauna (ammonites, belemnites, brachiopods, and plicatulids), although small bivalves and wood fragments are locally found. The upper Valanginian succession is interpreted as a transgressive-regressive sequence, the top of which is frequently eroded. The maximum depositional depth reached a rather deep outer shelf environment during the "middle" late Valanginian.
3. The uppermost Valanginian series (8–22 m) is mainly composed of marlstone, thin limestone beds, sandy limestone to the south, and of sandy marlstone and calcareous sandstone to the north. The succession exhibits an overall thinning-, then thickening-upward trend. The macrofauna is dominated by ammonites, belemnites, brachiopods, plicatulids, and serpulids, locally associated with gastropods and wood fragments. To the north and east of the basin, the uppermost Valanginian deposits are made of sandstone (**Zalidou**) locally showing current ripples, Hummocky Cross Stratification (HCS), and low angle lamination (Ida w Iddar) (Fig. 3), interpreted as foreshore deposits. This succession is thus interpreted as a transgressive-regressive sequence reaching an outer shelf environment to the south. The thick overlying Hauterivian marlstone represents a new, major sea level rise (Ferry et al., 2007).

4.2. Calcareous nannofossil biostratigraphy

The identified biozones of Bralower et al. (1995) and Sissingh (1977) are illustrated for the Zalidou section (Fig. 4), Ait Hamouch section (Fig. 5), and Hole 416A (Fig. 6). Secondary nannofossil bioevents were also observed (Figs. 4-6). Nannofossil zonal and subzonal markers are illustrated in Fig. 7.

A gradual size transition was observed between *Eiffelithus windii* and *E. striatus* (Applegate and Bergen, 1988; Bralower et al., 1989; Bown and

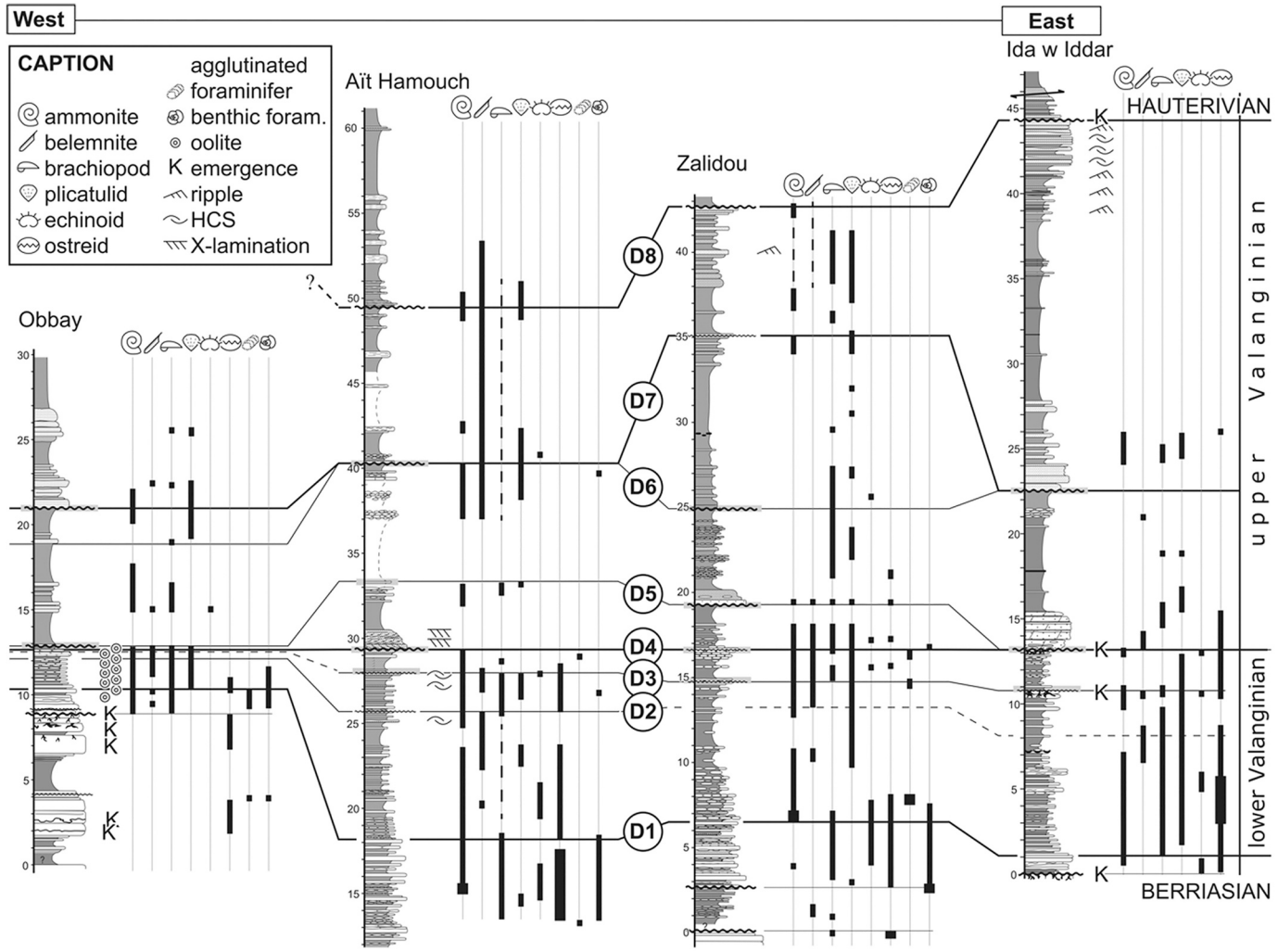

Fig. 3. Main sedimentary features, faunal assemblages, and discontinuities (D1 to D8) of some Valanginian sections in the Essaouira-Agadir Basin. Location of sections is shown in Fig. 1B.

Concheyro, 2004), making a proper differentiation difficult. Coccoliths with the length of their long-axes greater than 6.0 μm and with a relatively wide central area (almost 2/3 or greater of coccolith length) were identified in this study as *E. striatus* (Fig. 7).

Additionally, a new calcareous nannofossil biostratigraphy is proposed for Hole 416A. Čepek and Gartner (1980) dated the interval between cores 48–1 and 7–1 (~ −1530 to −1000 mbsf) to the early Valanginian-late Hauterivian based on calcareous nannofossil biostratigraphy. The LO of *R. wisei* was observed in this study in core 11–4 (−1200 mbsf; Fig. 6). In the Zalidou and Aït Hamouch sections, the LO of *R. wisei* was observed in the early late Valanginian (lower and upper *N. peregrinus* StZ in Zalidou and Aït Hamouch, respectively; Figs. 4, 5). Also, our results demonstrate that the Valanginian stage extends to core 9–3 (−1122 mbsf) based on the LO of *T. verenae* (top NK3B Subzone). In the onshore sections, the top of the NK3B Subzone ends in the late Valanginian (uppermost *N. peregrinus* StSz). The LO of *T. verenae* was also observed at a similar stratigraphic interval both in the Vocontian Basin (Duchamp-Alphonse et al., 2007; Gréselle et al., 2011) and in the Subbetic Basin (Aguado et al., 2018). Therefore, we can assume that the top of the studied interval at Hole 416A records the late Valanginian, but not the latest Valanginian.

4.3. Calcareous nannofossil assemblages

The majority of studied samples show good to moderate preservation of calcareous nannofossils with minor dissolution and recrystallization (Fig. 8). Note that the delicate structures of coccoliths are still visible. Highly dissolved and recrystallized coccoliths were limited to 14–18% of all the samples.

Following the abundance classes defined by Erba and Quadrio (1987), calcareous nannofossils are common (10–20 specimens per field of view) in the majority of the studied samples. The calcareous nannofossil assemblage is dominated by eight and nine groups of taxa in the onshore and offshore successions, respectively, illustrated in Fig. 7. Altogether, they constitute on average 81% of the total assemblage at Zalidou, 88% at Aït Hamouch, and 79% at Hole 416A. They are: *Watznaueria barnesiae/fossacincta*, *Diazomatolithus lehmanii/subbeticus*, small *Zeugrhabdotus* spp., *Biscutum ellipticum*, nannoconids, and to a lesser extent *Discorhabdus ignotus*, other *Watznaueria* species (*W. biporta* and *W. britannica*), and *Assipetra infracretacea*. *Rotelapillus crenulatus* are negligible in both onshore sections, but not at Hole 416A. The reader is referred to the Supplementary Table for more details.

In this study, *Diazomatolithus lehmanii* and *Diazomatolithus subbeticus* were combined since they are considered as morphological variants (Grün and Allemann, 1975). The small *Zeugrhabdotus* spp. in this study correspond to *Zeugrhabdotus* with long axis $\leq$ 5 μm combined with *Zeugrhabdotus erectus*. Finally, *W. barnesiae* and *W. fossacincta* were merged since they are considered to be morphological variants (Bornemann and Mutterlose, 2006).

The nannoconid group is mainly represented in all studied

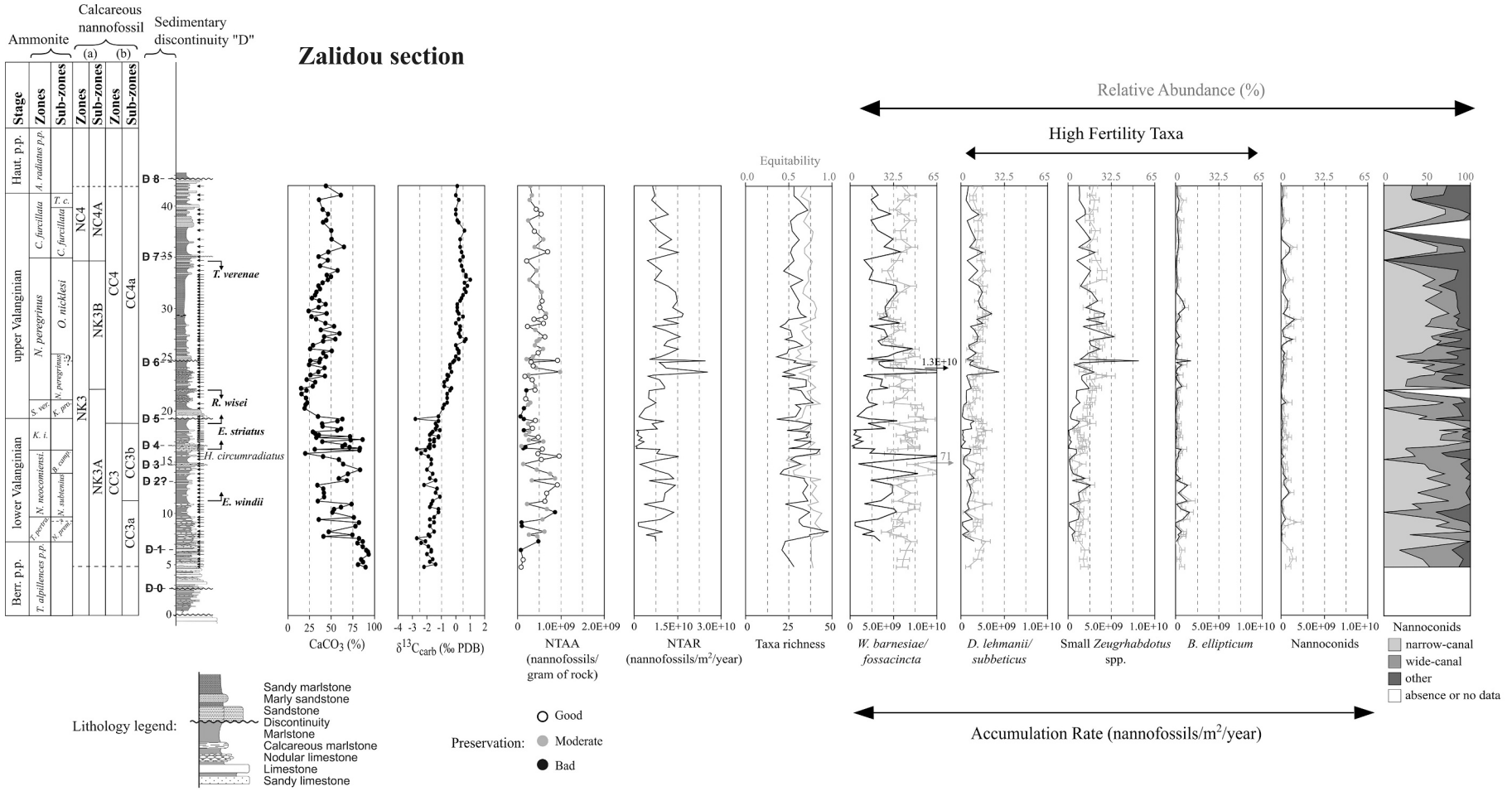

Fig. 4. Calcareous nannofossil and geochemical results in the Zalidou section. Sample locations are indicated by the arrow signs. The recognized stages are plotted with, the ammonite biostratigraphy (zones/subzones) following the ammonite standard zonation of the Mediterranean Province from Reboulet et al. (2018), calcareous nannofossil biostratigraphy (zones/subzones) following the (a) NC and NK zonation of Bralower et al. (1989, 1995) and (b) CC zonation of Sissingh (1977) modified by Applegate and Bergen (1988), sedimentary discontinuities (D0 to D8), and lithology. Calcareous nannofossil first and last occurrences are included; taxa indicated in "bold" font are used in the biostratigraphic schemes (a) and (b), and those in "normal" font correspond to the secondary bioevents. Binomial proportion confidence intervals are included for the nannofossil relative abundances using the 'exact' Clopper–Pearson method. The proportion of narrow- and wide-canal nannoconids within the nannoconid population are also shown, "other" nannoconids include specimens whose central-canal was not recognizable. Abbreviations: Berr., Berriasian; Haut., Hauterivian; *T. pertra.*, *T. pertransiens*; *N. prem.*, *N. premolicus*; *N. neocomiensi.*, *N. neocomiensiformis*; *B. camp.*, *B. campylotoxus*; *K. i.*, *K. inostranzewi*; *S. ver.*, *S. verrucosum*; *K. pro.*, *K. pronecostatum*; *T. c.*, *Teschenicera callidiscum*; NTAA, nannofossil total absolute abundance and NTAR, nannofossil total accumulation rate.

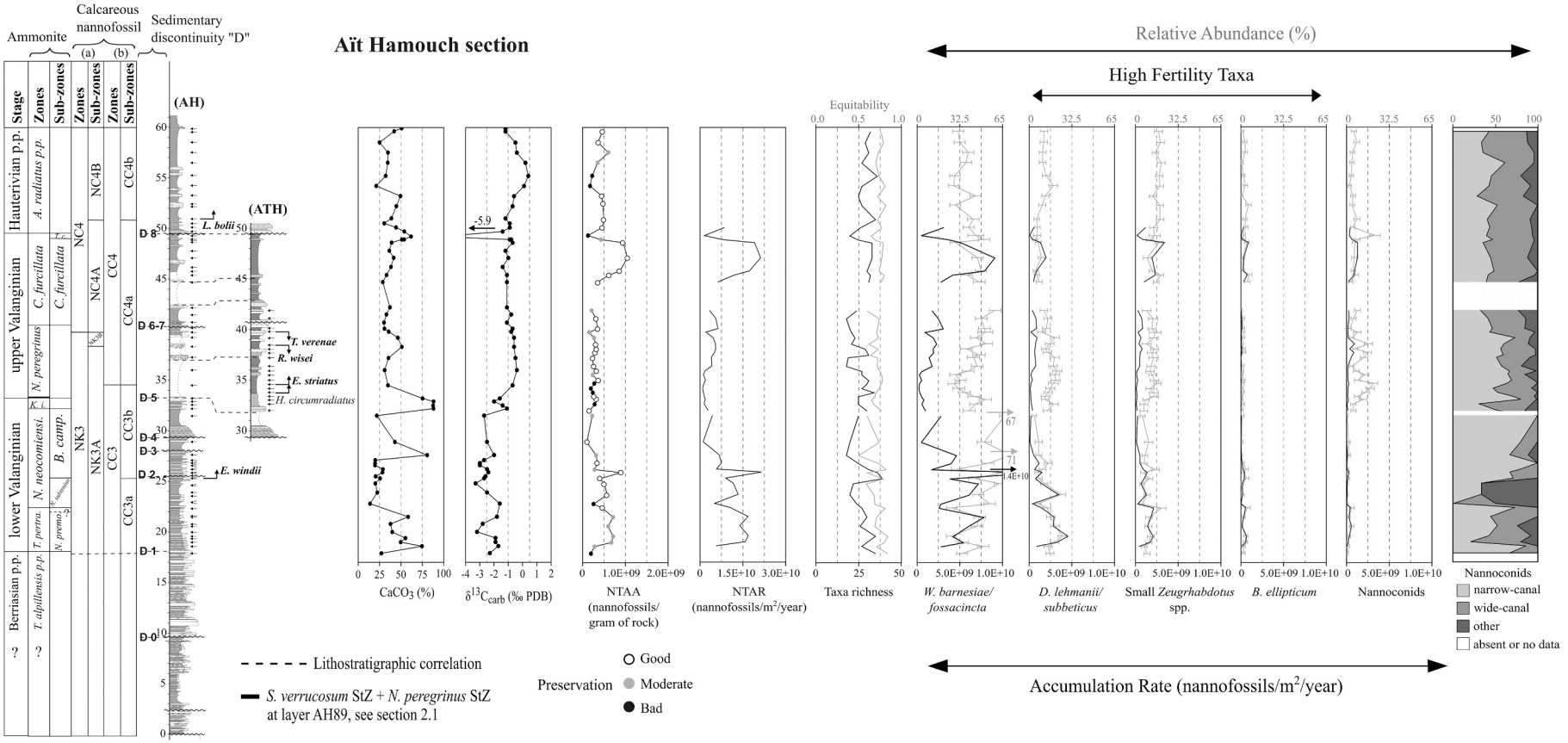

Fig. 5. Calcareous nannofossil and geochemical results in the Aït Hamouch section, same caption and lithology legend as for Fig. 4. Calcareous nannofossil results from "AH" section are separated from "ATH" section (see Section 2).

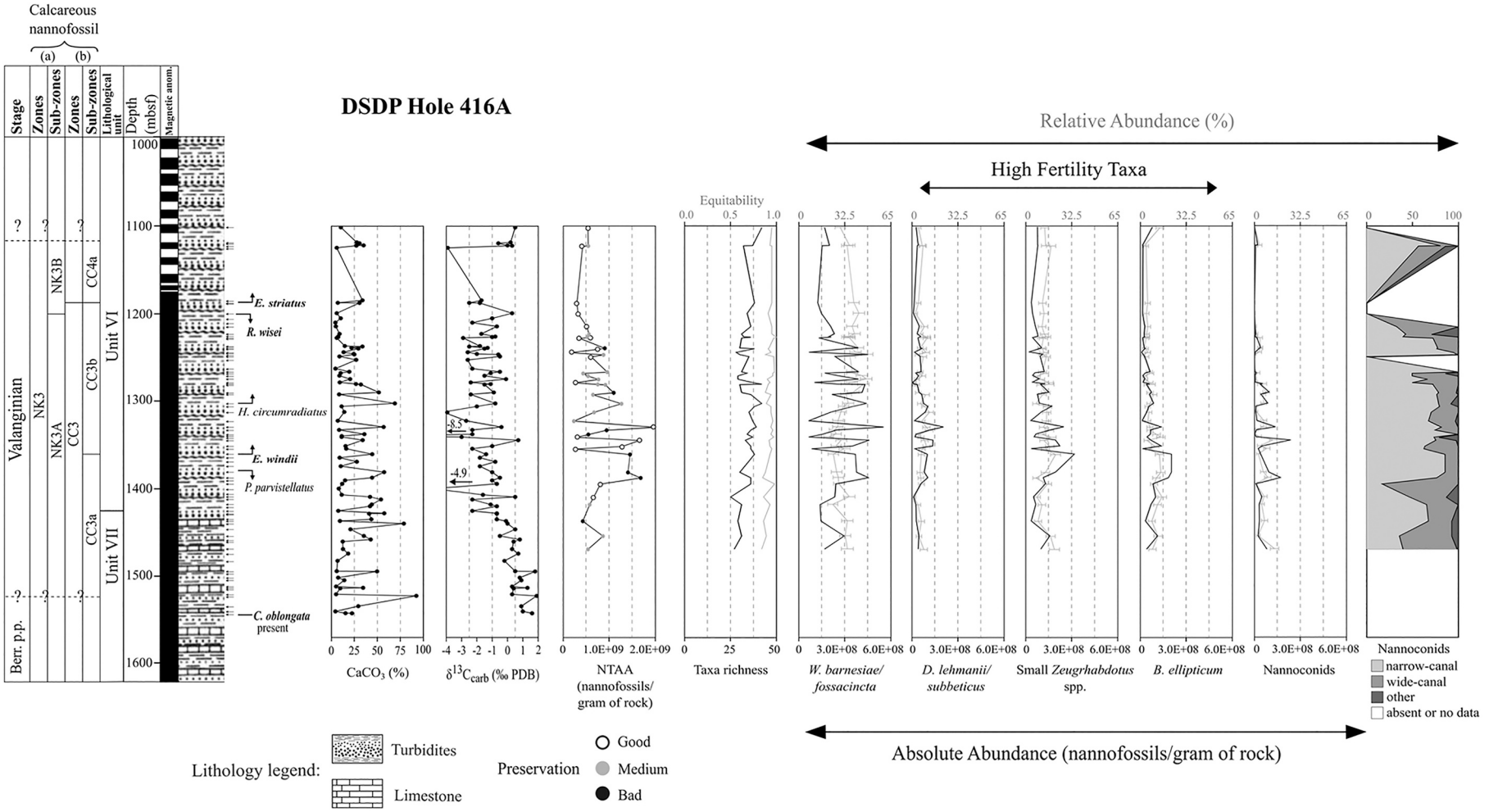

Fig. 6. Calcareous nannofossil and geochemical results in the DSDP Hole 416A. Sample locations are indicated by the arrow signs. The recognized stage is plotted with, the calcareous nannofossil biostratigraphy (zones/subzones) following the (a) NC and NK zonation of Bralower et al. (1989, 1995) and (b) CC zonation of Sissingh (1977) modified by Applegate and Bergen (1988), and lithology. Calcareous nannofossil first and last occurrences are included; taxa indicated in "bold" font are used in the biostratigraphic schemes (a) and (b), and those in "normal" font correspond to the secondary bioevents. Binomial proportion confidence intervals are included for the nannofossil relative abundances using the 'exact' Clopper–Pearson method. The proportion of narrow- and wide-canal nannoconids within the nannoconid population are also shown, "other" nannoconids include specimens whose central-canal was not recognizable. Abbreviations: Berr., Berriasian; magnetic anom., magnetic anomalies; and NTAA, nannofossil total absolute abundance.

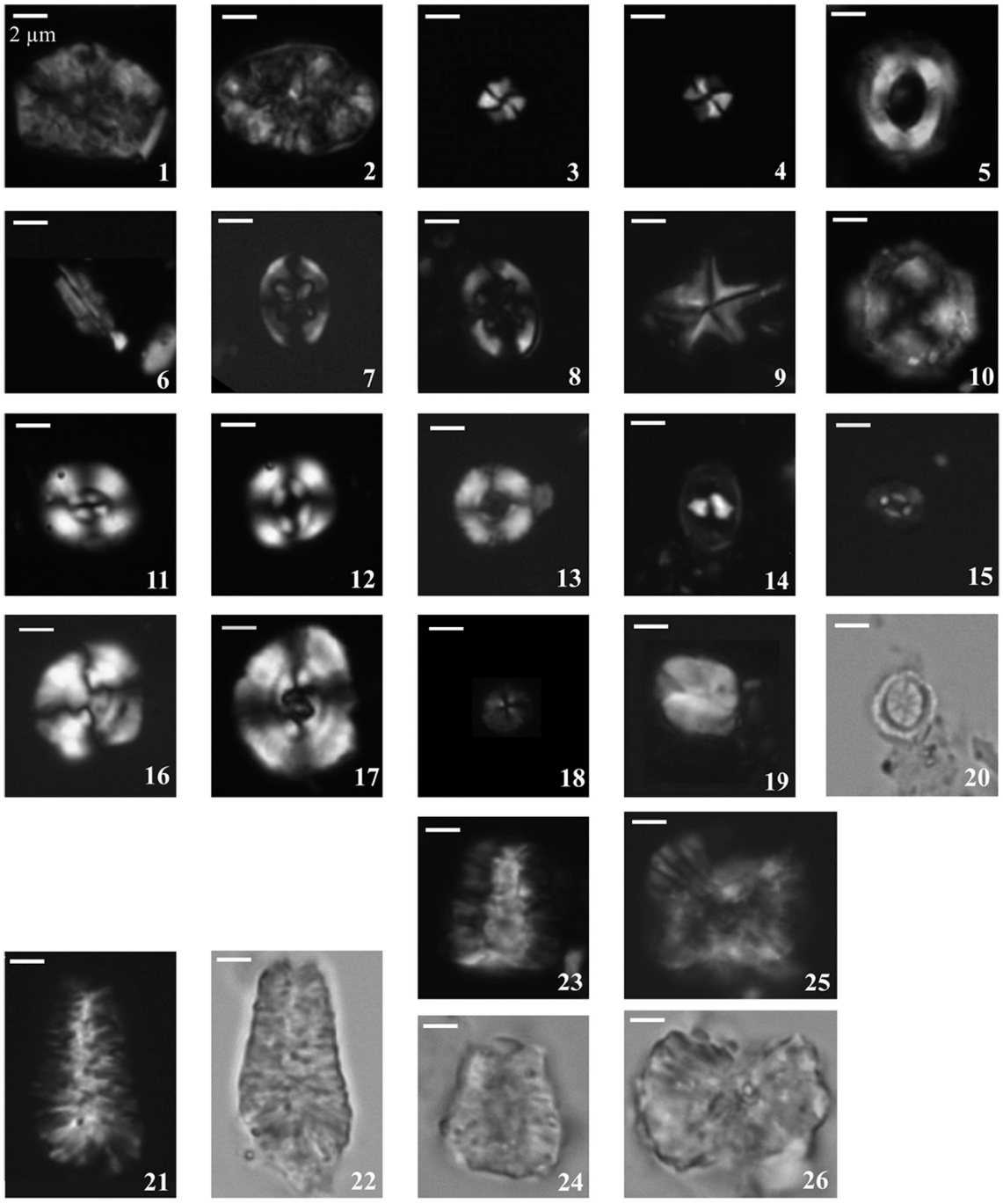

Fig. 7. Photomicrographs of the selected nannofossil species (XPL: cross-polarized light; PPL: plane-polarized light). 1, *Calcicalathina oblongata*, side view, XPL, sample Za43c; 2, *Calcicalathina oblongata*, top view, XPL, sample Za49b; 3, *Rucinolithus wisei*, XPL, sample Za27a; 4, *Rucinolithus wisei*, XPL, sample Za27a, same specimen rotated ~90°; 5, *Tubodiscus verenae*, XPL, sample 416A 21R2w 103–104; 6, *Lithraphidites bollii*, XPL, sample AH112a; 7, *Eiffellithus windii*, XPL, sample 416A 10R2w 144–145; 8, *Eiffellithus striatus*, XPL, sample Za53a; 9, *Polycostella parvistellatus*, XPL, sample 416A 49R1w 124–125; 10, *Haqius circumradiatus*, XPL, sample ATH2d; 11, *Watznaueria barnesiae*, XPL, sample Za28a; 12, *Watznaueria fossacincta*, XPL, sample Za39a; 13, *Diazomatolithus lehmanii*, XPL, sample Za32b; 14, *Zeugrhabdotus erectus*, XPL, sample 416A 9R3w 135–136; 15, *Biscutum ellipticum*, XPL, sample Za32a; 16, *Watznaueria biporta*, XPL, sample Za32a; 17, *Watznaueria britannica*, XPL, sample Za39c; 18, *Discorhabdus ignotus*, XPL, sample Za39d; 19, *Assipetra infracretacea*, XPL, sample Za32a; 20, *Rotelapillus crenulatus*, PPL, sample 416A 47R1w 76–77; 21, *N. steinmannii* subsp. *steinmannii*, XPL, sample ATH2h; 22, *N. steinmannii* subsp. *steinmannii*, PPL, sample ATH2h, same specimen; 23, *N. kamptneri* subsp. *minor*, XPL, sample ATH2f; 24, *N. kamptneri* subsp. *minor*, PPL, sample ATH2f, same specimen; 25, *N. globulus* subsp. *globulus*, XPL, sample ATH2f; 26, *N. globulus* subsp. *globulus*, PPL, sample ATH2f, same specimen.

successions by three taxa, *N. steinmannii* corresponding to narrow-canal, and *N. kamptneri* and *N. globulus* both corresponding to wide-canal (see Supplementary Table). These three taxa constitute on average ~ 80% of the total nannoconid population in both onshore sections and ~ 94% at Hole 416A. Additionally, *N. steinmannii* is the dominant taxon within the total nannoconid population in all three successions (see Supplementary Table).

4.3.1. Calcareous nannofossil absolute abundance and accumulation rate

Four and three intervals with different sedimentation rates were identified throughout the Valanginian stage in Zalidou and Aït Hamouch, respectively (see Supplementary Table). Thus, allowing the

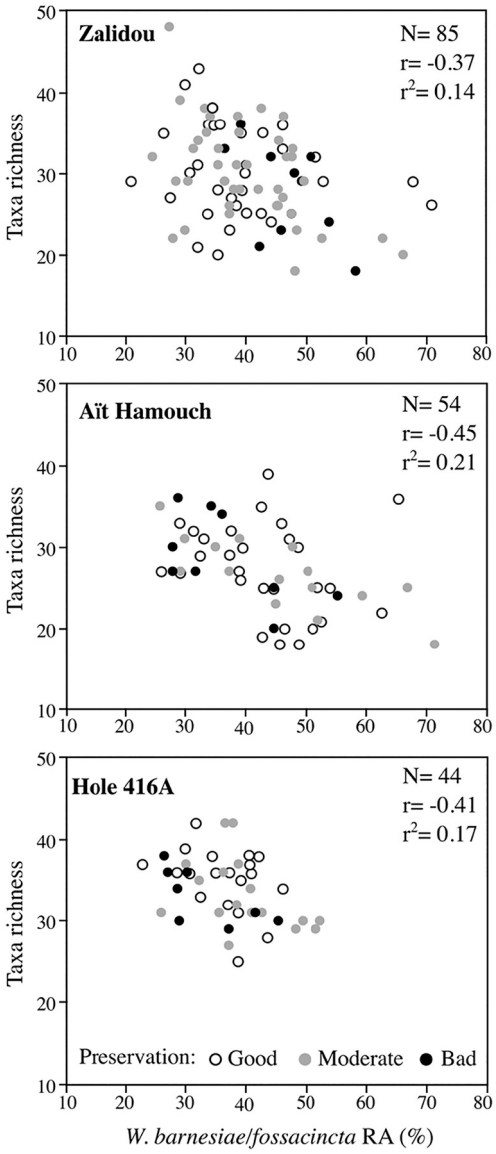

Fig. 8. Plot of *W. barnesiae/fossacincta* relative abundance (RA, %) and taxa richness in Zalidou, Aït Hamouch, and Hole 416A samples. Preservation classes follow the classes defined by Roth and Thierstein (1972) and modified by Roth (1983). N is the total number of samples, r and r^2 are the correlation coefficients.

calculation of the nannofossil total accumulation rate (NTAR, nannofossils/m^2/year). It was not possible to calculate sedimentation rates, and then NTAR, for Hole 416A because the large scatter in $\delta^{13}C_{carb}$ (Fig. 6) hindered identifying possible correlation points with the $\delta^{13}C_{carb}$ curve from Martinez et al. (2015).

The average nannofossil total absolute abundance (NTAA, nannofossils/gram of rock) is higher offshore compared to onshore, and the average NTAR is higher at Zalidou than at Aït Hamouch (Figs. 4–6, see also Supplementary Table). In both Zalidou and Aït Hamouch successions (Figs. 4 and 5), the NTAR is high in the early Valanginian. Afterwards, NTAR decreases and minimal values are recorded around the early-late Valanginian transition (*K. inostranzewi* to *S. verrucosum* StZ, upper NK3A and upper CC3b subzones). Upwards, in the late Valanginian, NTAR gradually increases in both successions. It reaches maximal values within the *N. peregrinus* StZ at Zalidou (Fig. 4), followed by a slight decrease during the rest of the succession. At Aït Hamouch, NTAR values higher than that of the early Valanginian are recorded within the *C. furcillata* StZ (Fig. 5). In both successions, NTAR reflects an amplification of NTAA with very similar trends (Figs. 4 and 5), which implies that the sedimentation rate does not significantly affect the NTAA. At Hole 416A, NTAA is low in the lower NK3A and CC3a subzones, and increases during the mid-NK3A and upper CC3a to lower CC3b subzones (Fig. 6). Thereafter, the NTAA gradually decreases to minimal values in the NK3B and the CC3b-CC4a subzones transition.

In this study, only the taxa that presented significant variations in all studied successions are considered (Figs. 4–6). Thereby, the following groups are not described: other *Watznaueria* species (*W. biporta* and *W. britannica*), *A. infracretacea*, *D. ignotus*, and *R. crenulatus*. For Zalidou and Aït Hamouch sections, the absolute abundance (AA, nannofossils/gram of rock) of nannofossil taxa are shown in Figs. Supp. 2 and 3, respectively (see also Supplementary Table). The average accumulation rate (AR, nannofossils/m^2/year) of each considered nannofossil taxon is generally higher at Zalidou (Fig. 4) compared to Aït Hamouch (Fig. 5), except for nannoconids their average AR is higher at Aït Hamouch than at Zalidou (Supplementary Table).

The AR of nannofossil taxa in the onshore sections generally decreases during the *B. campylotoxus* LSz and *K. inostranzewi* StZ (NK3A and lower CC3b subzones), earlier than the decrease of NTAR. Their AA in Hole 416A decreases during the same calcareous nannofossil subzones. Notably, the reductions in the NTAR and the AR of taxa are observed earlier in Aït Hamouch (*B. campylotoxus* LSz) with respect to Zalidou (*K. inostranzewi* StZ). During the rest of the successions, the AR or AA of nannofossil taxa generally follow the same trend as that of the NTAR or NTAA, respectively (Figs. 4–6).

4.3.2. Calcareous nannofossil diversity indices and relative abundances

Taxa richness and equitability are plotted for Zalidou (Fig. 4), Aït Hamouch (Fig. 5), and Hole 416A (Fig. 6). The offshore succession is characterized by higher nannofossil diversity indices compared to those of the onshore sections. At Zalidou (Fig. 4), the taxa richness shows a long-trend decrease from the early to late Valanginian. The equitability is highest in the early Valanginian. At Aït Hamouch (Fig. 5), the taxa richness decreases to lowest values in the late early Valanginian and in the early late Valanginian. The lowest equitability values are recorded in the late early Valanginian. At Hole 416A (Fig. 6), both taxa richness and equitability increase during the lower NK3A and CC3a to lower CC3b subzones. Upwards, the equitability remains high in the rest of the Valanginian, whereas the richness decreases.

At Zalidou (Fig. 4), the RA of *W. barnesiae/fossacincta* is high in the early Valanginian and around the early-late Valanginian transition, then it decreases during the early late Valanginian. At Aït Hamouch (Fig. 5), its RA increases during the late early Valanginian and during the late Valanginian. The RA of *D. lehmanii/subbeticus* increases at Zalidou in the late Valanginian and remains high upsection. Whereas, its RA at Aït Hamouch decreases in the late early Valanginian, followed by a re-increase in the early late Valanginian. In both onshore sections, the RA of small *Zeugrhabdotus* spp. increases to highest values in the late Valanginian. The RA of *B. ellipticum* decreases in both onshore sections to minimal values from the late early Valanginian. Its RA re-increases only at Aït Hamouch in the late Valanginian. The RA of nannoconids declines to minimal values in Zalidou (Fig. 4) from the late early Valanginian to the early late Valanginian. Whereas, at Aït Hamouch (Fig. 5), the RA of nannoconids is low in the early Valanginian and increases to maximal values in the early late Valanginian. A change in the proportion of narrow-canal nannoconids within nannoconid population is observed at Aït Hamouch. Their proportion is high from the early Valanginian to the early late Valanginian compared with the rest of the Valanginian (Fig. 5).

At Hole 416A (Fig. 6), the RA of *W. barnesiae/fossacincta* increases during the upper NK3A and CC3b subzones. The RA of *D. lehmanii/subbeticus* is relatively stable throughout the Valanginian. The RA of small *Zeugrhabdotus* spp. increases during the upper NK3A and CC3b subzones. The RA of *B. ellipticum* decreases during the same biozones. The RA of nannoconids decreases in the upper NK3A to NK3B and upper

CC3b to CC4a subzones. The proportion of narrow-canal nannoconids within the nannoconid population is generally lower in the lower NK3A and CC3a subzones compared with the rest of the succession.

4.4. Calcium carbonate content and carbon isotopes

The $CaCO_3$ (%) contents range between 15 and 93 (avg. 49%) at Zalidou, 14–88 (avg. 41%) at Aït Hamouch, and 4–92 (avg. 23%) at Hole 416A. At both onshore sections (Figs. 4 and 5), the highest $CaCO_3$ content is recorded in the early Valanginian. At Zalidou, the decrease in $CaCO_3$ content is concomitant with a lithological change to more clastic-rich marlstone-limestone beds. At Hole 416A (Fig. 6), the $CaCO_3$ content decreases and exhibits fewer fluctuations in the upper NK3A to NK3B and upper CC3b to CC4a subzones, compared with down-section.

The $\delta^{13}C_{carb}$ values range between −2.8 and + 1 (avg. –0.8‰) at Zalidou, −3.3 and + 0.4 (avg. –1.5‰) at Aït Hamouch, and between −4.9 and + 1.9 (avg. –1.0‰) at Hole 416A. At Zalidou (Fig. 4), the $\delta^{13}C_{carb}$ increases from −2.4‰ to +1‰ between the latest early Valanginian (*K. inostranzewi* StZ, upper NK3A, and upper CC3b subzones) and the latest Valanginian (upper *O. nicklesi* StSz, upper NK3B, and upper CC4a subzones). At Aït Hamouch (Fig. 5), the $\delta^{13}C_{carb}$ increases from ∼ −2.5‰ to ∼ −0.4‰ between the latest early Valanginian (*K. inostranzewi* StZ, upper NK3A, and upper CC3b subzones) and the early late Valanginian (lower *N. peregrinus* StZ, upper NK3A, and lower CC4a subzones). Accordingly, the carbon-isotope positive shift is of magnitude 3.7‰ and 2.3‰ at Zalidou and Aït Hamouch, respectively. Then, the $\delta^{13}C_{carb}$ smoothly decreases in the rest of the late Valanginian in both, Zalidou (∼ +0.1‰) and Aït Hamouch (∼ −1.1‰). At Hole 416A, the $\delta^{13}C_{carb}$ does not show any positive shift (Fig. 6).

5. Interpretation

5.1. Sedimentary paleoenvironment

Except in the lower Valanginian condensed strata of the Obbay section, we did not observe oolites in the limestone beds. This indicates a rather low energy depositional environment in the EAB during most of the Valanginian. As a matter of fact, since trade winds blew to the west, and because the EAB is located on the western coast of Africa, it was little affected by intense tropical storms. These storms may have been generated in the Atlantic Ocean, but were pushed to the west by the trade winds and to the north by the Coriolis force (see Trabucho Alexandre et al., 2011; Pohl et al., 2019; Jaillard et al., 2021). Therefore, the EAB can be considered to have been a low energy ramp gently sloping toward the ocean. However, the numerous oolites observed on the Obbay swell (Fig. 3) indicate that the shallowest part of the water column was moderately agitated, at least in the early Valanginian. Actually, in the sandstone and sandy limestone beds of late early and late Valanginian age, ripples and scarce trough cross beds indicate a moderate wave activity, while planar parallel laminations suggest tidal processes. Also, the occurrence of thin-bedded HCS in shallow marine beds suggests the occurrence of storms of low intensity. During the late early Valanginian and late Valanginian, the moderate hydrodynamic activity of the surficial part of the water column also accounted for the occurrence of sandstone or sandy limestone beds above the surfaces interpreted as sequence boundaries (Fig. 3). This may be due to the erosion occurring during low sea-level periods, which removed the shale particles and cleared up quartz grains from the sediments. The quartz grains were then deposited as sandy beds during the subsequent transgression.

The scarcity of corals and algae, the abundance of agglutinated foraminifers, and the presence of bryozoans in the calcareous beds (mainly early Valanginian) suggest temperate to cold sea water temperatures. Because of the activity of trade winds, the EAB was probably subjected to upwellings (Price et al., 1995; Poulsen et al., 1998). Oceanic upwellings may explain both the cold to temperate waters, and the common occurrence of phosphate in shallow deposited beds.

The abundance of ostreids and plicatulids throughout the section suggests mesotrophic conditions, while the presence of agglutinated foraminifers in the early Valanginian suggests, additionally, an oxygen depletion at that time (e.g., Kuhnt et al., 1996; Reolid et al., 2008; Kender and Kaminski, 2017). This interpretation is supported by the abundance of pyrite in the lower Valanginian marlstone of the southern sections. Oxygen depletion, however, must have been mild or sporadic since echinoids are common at that time. Mesotrophic conditions were most likely related to the terrigenous influx of fine-grained clastic particles, more abundant toward the north and east (Fig. 9). This is supported by the sporadic occurrence of wood and leaf fragments (Zalidou) in Valanginian deposits. Actually, a combination of high terrigenous supply, temperate to cold temperature, and the presence of upwellings favor the development of heterozoan carbonate systems (Michel et al., 2018).

5.2. Paleogeography

In the early Valanginian, the northern sections were marked by open marine, oyster-rich shallow carbonate shelf facies exhibiting several karstified surfaces. Whereas, the southern ones presented distal facies marked by thick marlstone intervals, abundant cephalopods, and the lack of emergence evidence (Fig. 9). During the late Valanginian, the northern sections recorded the progradation of a clastic sedimentary system (Fig. 9), which indicates that the clastic supply proceeded from the Central High Atlas (Ferry et al., 2007). Clastic supply was interrupted by a significant erosion period (D7, Figs. 3 and 9), likely related to an emergence episode. Furthermore, the uppermost Valanginian deposits end up with foreshore deposits and are capped by an emergence surface to the northeast (Ida w Iddar). Conversely, the coeval sediments in Zalidou bear cephalopods and plicatulids, and end up with a submarine erosional surface to the southwest (Aït Hamouch). The southwestward sloping topography is supported by the onlap of the lower upper Valanginian sequence to the north or northeast (Fig. 3). Although sandstone prograded in the northern part of the basin during the late Valanginian, the southernmost section (Aït Hamouch) displays sandy layers in the late early to earliest late Valanginian (Fig. 9). This suggests that the course of rivers that supplied quartz grains to the EAB was changing through time.

In the Obbay section, the lower Valanginian succession is very condensed (Fig. 3). Two explanations may be proposed. First, the presence of strong upwelling currents in the early Valanginian (Price et al., 1995; Poulsen et al., 1998) could have accounted both for the condensation and the abundance of phosphate and glauconite (Föllmi, 1996; Puhfal and Groat, 2017). Second, incipient movements of the Amsittene diapir (e.g., Tari and Jabour, 2013) or compressional tectonics in Early Cretaceous times (Bertotti and Gouiza, 2012; Fernández-Blanco et al., 2020) may have locally uplifted this area. If so, the area became a shallow swell reaching the Fair-Weather Wave Base, on which a high energy regime caused condensation. A combination of both upwelling and uplift is likely. The fact that condensation disappears during the late Valanginian sea level rise suggests that either, upwelling currents were less active, or more probably, their activity was distributed and mitigated in the thicker water column.

5.3. Preservation of a calcareous nannofossil primary signal

The relative abundance (RA) of the solution-resistant *W. barnesiae/fossacincta* taxa is used as an indication of the preservation state. Roth and Krumbach (1986) suggested that relative abundances of *W. barnesiae* > 40% indicate high degree of diagenesis and dissolution, while Williams and Bralower (1995) suggested that even higher proportions (> 70%) indicate assemblage alteration. In the studied samples, the RA of *W. barnesiae/fossacincta* is on average 41% at Zalidou, 43% at Aït Hamouch, and 37% at Hole 416A. Additionally, RA ranges of *W. barnesiae/fossacincta* in this study are not very different from those

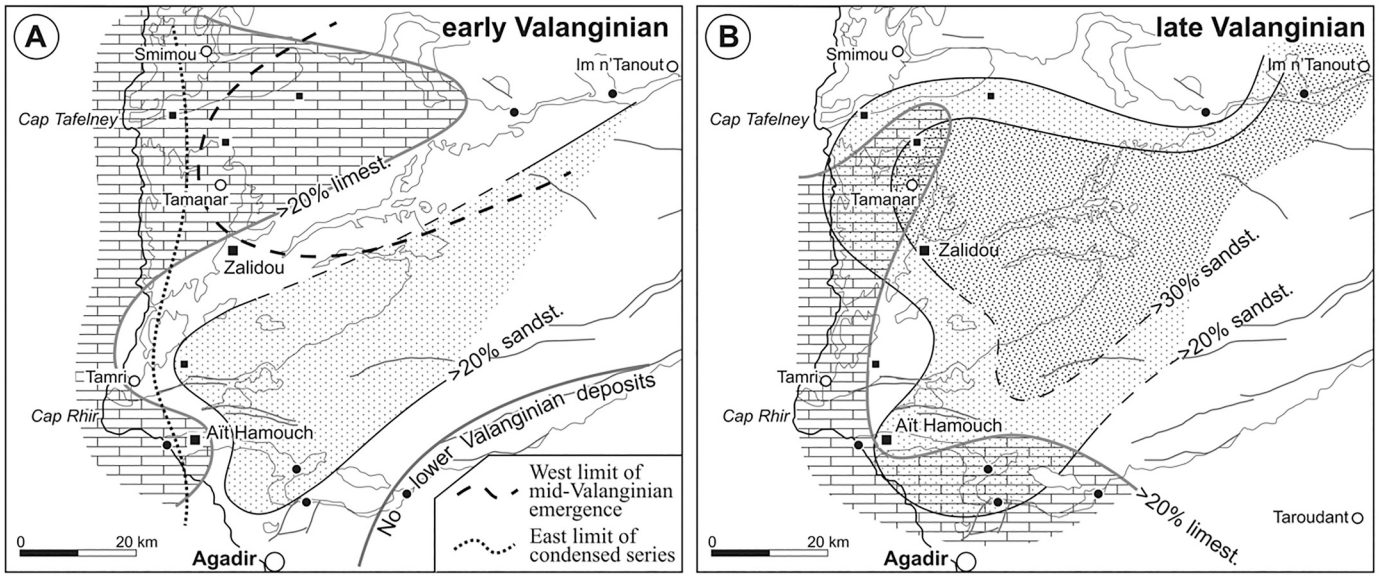

Fig. 9. Paleogeographic sketch of the Essaouira-Agadir Basin showing the distribution of sandstone and limestone in the (A) lower Valanginian and the (B) upper Valanginian deposits. Reconstruction based on data from this study (black squares) and from Ferry et al. (2007) (black dots).

recorded in other basins: ~50–90% in the Lombardian and Belluno Basins-northern Italy (Erba and Tremolada, 2004); 48–78% in the Vocontian Basin, SE France (Reboulet et al., 2003); 18–77% in DSDP Site 535, Gulf of Mexico (Kessels et al., 2006); and 22–59% in DSDP Hole 603B, northern Atlantic (Bornemann and Mutterlose, 2008). Also, *W. barnesiae/fossacincta* dominate the assemblage in the Subbetic Domain (SE Spain) although no quantification was done (Aguado et al., 2018). Most of these studies come from sections having experienced low levels of diagenesis, supporting that the dominance of *W. barnesiae/fossacincta* is not a local effect.

The correlation between the RA of *W. barnesiae/fossacincta* and the taxa richness was tested in all the studied successions (Fig. 8). Despite the fact that a negative correlation can be suspected ($r = -0.37$, $p_{uncorr.} = 0.0005$, $n = 85$ in Zalidou; $r = -0.45$, $p_{uncorr} = 0.0006$, $n = 54$ in Aït Hamouch; and $r = -0.41$, $p_{uncorr} = 0.005$, $n = 44$ in Hole 416A), the preservation classes show that samples with strong dissolution and recrystallization do not necessarily correspond to high proportions of *W. barnesiae/fossacinta* (Fig. 8). These samples are homogenously distributed for any given proportion of *W. barnesiae/fossacinta*. Moreover, some samples with good and moderate preservation present a high percentage (> 40%) of *W. barnesiae/fossacincta*, which implies that the high proportions of *W. barnesiae/fossacincta* can also be part of the original calcareous nannofossil assemblage during the Valanginian.

Thereby, based on all aforementioned evidence, we assume that the nannofossil assemblages of both the Essaouira-Agadir Basin and the DSDP Hole 416A are slightly affected by diagenetic alteration but still hold a primary signal that can be used for the paleoceanographic reconstruction.

5.4. Time succession in calcareous nannofossil assemblages

The nannofossil total accumulation rate (NTAR) and nannofossil total absolute abundances (NTAA) along with the accumulation rate (AR), absolute abundance (AA), and relative abundance (RA) of the major calcareous nannofossil taxa demonstrate variations from the early to late Valanginian. This, associated with the sedimentology results, will allow the reconstruction of the paleoceanographic conditions on the central Moroccan margin and to better constrain the evolution of paleoceanographic conditions around the Weissert Event. As the late Berriasian *p.p.* was only recognized at Zalidou and the early Hauterivian *p.p.* was only recognized at Aït Hamouch, the discussion will be focused on paleoceanographic conditions during the Valanginian.

For the paleoceanographic reconstruction, the NTAR (and NTAA for Hole 416A) is used as a proxy to estimate the nannofossil production. The accumulation rates and abundances (absolute and relative) of the selected nannofossil taxa are used as a proxy for surface-water fertility levels. The ecological affinity of calcareous nannofossil taxa used for this purpose, along with the associated literature, are summarized in Table 1.

5.4.1. The Zalidou section

During the early Valanginian (*N. premolicus* StSz to upper *B. campylotoxus* LSz, NK3A and upper CC3a to lower CC3b calcareous nannofossil subzones), except for small fluctuations the nannofossil production did not vary and was relatively high (Fig. 4). During the *N. premolicus* StSz and *N. subtenuis* LSz (lower NK3A and CC3a to lower CC3b subzones), favorable surface-water conditions allowed the development of the nannofossil community as suggested by the highest diversity indices. Additionally, local mesotrophic conditions are suggested by the abundant high-fertility taxa. Afterwards, a decoupling between NTAR, diversity indices, AR, and RA of the selected taxa is recorded. In the *B. campylotoxus* LSz (within the NK3A and CC3b subzones), surface-water conditions became less favorable, leading to a decrease in the AR of all nannofossil taxa and in the diversity. Only the eurytopic *W. barnesiae/fossacincta* remained high during this time interval, and the nannofossil production was maintained (Fig. 4).

In the latest early Valanginian (*K. inostranzewi* StZ, upper NK3A and upper CC3b subzones), the nannofossil production collapsed as supported by both, minimal NTAR and minimal AR of all nannofossil taxa (Fig. 4). Excluding poor preservation, this collapse could be explained by major paleoenvironmental changes.

Afterwards, in the late Valanginian (*S. verrucosum* to upper *O. nicklesi* StSz, upper NK3A to NK3B and uppermost CC3b to lower CC4a subzones), the nannofossil production gradually increased, supported by the re-increasing NTAR and AR of all nannofossil taxa (Fig. 4). The end of this recovery phase was marked by a high nannofossil production and meso-eutrophic conditions. The meso-eutrophic conditions are interpreted from the important increase in the small *Zeugrhabdotus* spp. during the late Valanginian (upper *N. peregrinus* and upper *O. nicklesi* StSz, NK3B and CC4a subzones). This time interval was also characterized by the recovery of nannoconids (Fig. 4).

Lastly, in the remaining late Valanginian, the nannofossil production slightly decreased with similar magnitudes as those observed in the early

Table 1
Main ecological affinity of the calcareous nannofossil taxa used for paleoceanographic reconstruction, following the specified literature.

Taxa	Fertility of surface waters	Ecological strategy	Paleoceanography
B. constans	eutrophic[5, 18, 19, 24, 25, 26, 27, 28, 29, 32, 33]	low diversified assemblages[18]	upwelling[5, 18, 24, 25, 26, 27, 28]
	meso-eutrophic[8]	eurytopic[17]	shelf surface-waters[21, 29]
B. ellipticum	eutrophic[9, 27] meso-eutrophic[16]	r-selected[18]	upwelling[6, 12, 30]
D. lehmanii	eutrophic[1, 4, 14, 20, 31, 33]		transgressive intervals[4] upwelling[33]
D. subbeticus	eutrophic[14]		distal environments[14]
nannoconids	oligotrophic[1, 2, 3, 7, 11, 18]	r-selected[29]	neritic[10, 25, 27, 28, 29]
	meso-oligotrophic[22]		lower photic zone[2, 7]
W. barnesiae	oligotrophic[8, 10, 11, 26, 28, 30, 31, 32]	eurytopic[13, 15, 21, 29]	oceanic setting[27]
	mesotrophic[23] eurytrophic[14]	r-selected[12, 23, 30]	
W. barnesiae/ fossacincta		eurytopic[13]	
Z. erectus	eutrophic[5, 9, 10, 11, 24, 25, 26, 27, 28, 29, 32, 33]	r-selected[6, 12, 23]	upwelling[5, 24, 25, 26, 27, 28]
	more eutrophic than *B. constans*[6]	low diversified assemblages[18]	shelf-surface water[18]
Small *Zeugrhabdotus* spp.	eutrophic[6, 32]		

1. Bersezio et al. (2002); 2. Bornemann et al. (2003); 3. Coccioni et al. (1992); 4. Crux (1989); 5. Erba (1992); 6. Erba et al. (1992); 7. Erba (1994); 8. Eleson and Bralower (2005); 9. Giraud et al. (2003); 10. Herrle (2002); 11. Herrle et al. (2003); 12. Lees (2002); 13. Lees et al. (2005); 14. Mattioli et al. (2014); 15. Mutterlose (1991); 16. Mutterlose (1992a); 17. Mutterlose (1992b); 18. Mutterlose and Kessels (2000); 19. Mutterlose et al. (2003); 20. Mutterlose et al. (2005); 21. Noël et al. (1987); 22. Pauly et al. (2012); 23. Pittet and Mattioli (2002); 24. Premoli Silvá et al. (1989); 25. Roth (1981); 26. Roth (1989); 27. Roth and Bowdler (1981); 28. Roth and Krumbach (1986); 29. Street and Bown (2000); 30. Thierstein (1980); 31. Tremolada et al. (2006); 32. Watkins (1989); 33. Williams and Bralower (1995).
B. ellipticum is considered as a morphotype of *B. constans* (Bornemann and Mutterlose, 2006).

Valanginian. However, despite a decrease in surface-water fertility, the fertility remained higher with respect to the early Valanginian as supported by the higher RA of the small *Zeugrhabdotus* spp. (Fig. 4).

5.4.2. The Aït Hamouch section

During the early Valanginian (*N. premolicus* StSz to *N. subtenuis* LSz, lower NK3A and CC3a to lowermost CC3b calcareous nannofossil subzones), the nannofossil production was high with values higher compared to the Zalidou section (Figs. 4 and 5). A decoupling between NTAR, diversity indices, AR, and RA of the selected nannofossil taxa is also observed (Fig. 5). During the *N. premolicus* StSz (lower NK3A and CC3a subzones), mesotrophic conditions in surface waters and a thick photic zone allowed a diverse calcareous nannofossil community to flourish. Also, these conditions allowed the development of benthic carbonate producers, such as agglutinated foraminifers, ostreids, and plicatulids (see Section 4.1). Afterwards, during the *N. subtenuis* LSz, the surface-water conditions became less favorable for both high-fertility taxa and nannoconids. As at Zalidou, the eurytopic *W. barnesiae/fossacincta* remained high during this time interval and nannofossil production was maintained (Fig. 5).

During the late early Valanginian (*B. campylotoxus* LSz to *K. inostranzewi* StZ, NK3A and CC3b subzones), the nannofossil production gradually declined and collapsed (Fig. 5). Excluding poor preservation, the trigger of the collapse can be also explained by major paleoenvironmental changes. Decline in the nannofossil production is suggested from the drastic decrease in accumulation rate and abundance of the dominant taxa, *W. barnesiae/fossacincta*. Nannofossil production remained low during the early late Valanginian (lower *N. peregrinus* StZ, upper NK3A Subzone and CC3a-CC3b subzones transition; Fig. 5). Decreasing percentages of *W. barnesiae/fossacincta* within the nannofossil assemblage explain that all other taxa show increasing percentages (in particular nannoconids) despite decreasing AR.

Afterwards, in the late Valanginian (upper *N. peregrinus* to *C. furcillata* StZ, upper NK3A to NC4A and CC4a subzones), the nannofossil production first recovered before reaching higher magnitudes than that of the early Valanginian (Fig. 5). This is attested by the increasing NTAR, and AR of all taxa. In parallel, enhanced surface-water trophic levels are demonstrated by the increasing abundances of both *D. lehmanii/subbeticus* and small *Zeugrhabdotus* spp.. The nannoconid AR is maximal, and is associated with decreasing proportion of narrow-canal forms (Fig. 5). Lastly, in the latest Valanginian (*T. callidiscum* StSz, uppermost NC4A and CC4a subzones), the nannofossil production and trophic levels decreased to magnitudes slightly lower than that of the early Valanginian.

5.4.3. DSDP Hole 416A

The lower NK3A and CC3a calcareous nannofossil subzones are characterized by an increase in the nannofossil production, as suggested by both increasing NTAA and abundances of meso-eutrophic taxa (Fig. 6). Marine conditions were also favorable for the development of nannoconids, as their absolute abundance is higher compared with both onshore sections (Fig. 6, and Figs. Supp. 2–3). In addition, the nannoconids were mainly represented by narrow-canal forms with the large dominance of *N. steinmannii* (Fig. 6). The assumption that narrow-canal *Nannoconus* inhabited the deep photic zone under stratified waters and a deep nutricline (Erba, 2004, 1994) has been challenged by Mattioli et al. (2014), who showed that *N. steinmannii* could have affinity for destratified surface waters. Hole 416A is characterized by turbiditic sequences and low calcium carbonate contents within the Valanginian sediments. The repeated input of clastic material would prevent the stratification of the water column.

Upsection, in the upper NK3A-NK3B and CC3b-CC4a subzones, the NTAA and AA of all taxa decrease (Fig. 6). Reduced surface-water fertility during this time interval is shown by the decreasing relative abundance of high-fertility taxa. Nannoconids decline slightly after the fertility decreased in the uppermost NK3A and upper CC3b subzones. These are interpreted as unfavorable surface-water conditions, similar to those observed in the onshore Essaouira-Agadir Basin.

The onset of the nannofossil production recovery, similar to that of NTAR observed onshore, seems to occur in the topmost samples (Fig. 6). However, the recovery phase itself as recorded in the onshore settings seems to be missing at Hole 416A.

5.5. The carbon isotope record and identifying the Weissert Event

At Zalidou, we identify the Weissert Event from the base of the carbon-isotope (CI) positive shift (16.25 m) until the climax (32.8 m; Fig. 10), following the formal definition of Erba et al. (2004). The CI positive shift is observed from the lower part of the *K. inostranzewi* StZ to the upper part of the *O. nicklesi* StSz (upper NK3A to upper NK3B and upper CC3b to upper CC4a calcareous nannofossil subzones). The top of the Weissert Event is recorded just below the LO of the nannofossil biomarker *T. verenae*.

At Aït Hamouch, the *S. verrucosum* StZ and the *O. nicklesi* StSz are not recognized (see Section 2.1). Additionally, the *N. peregrinus* StZ is reduced (~7 m) compared with Zalidou (~14 m). This can be also observed from the reduced NK3B calcareous nannofossil Subzone in Aït Hamouch (1.5 m) compared with Zalidou (12.5 m; Fig. 10). Moreover,

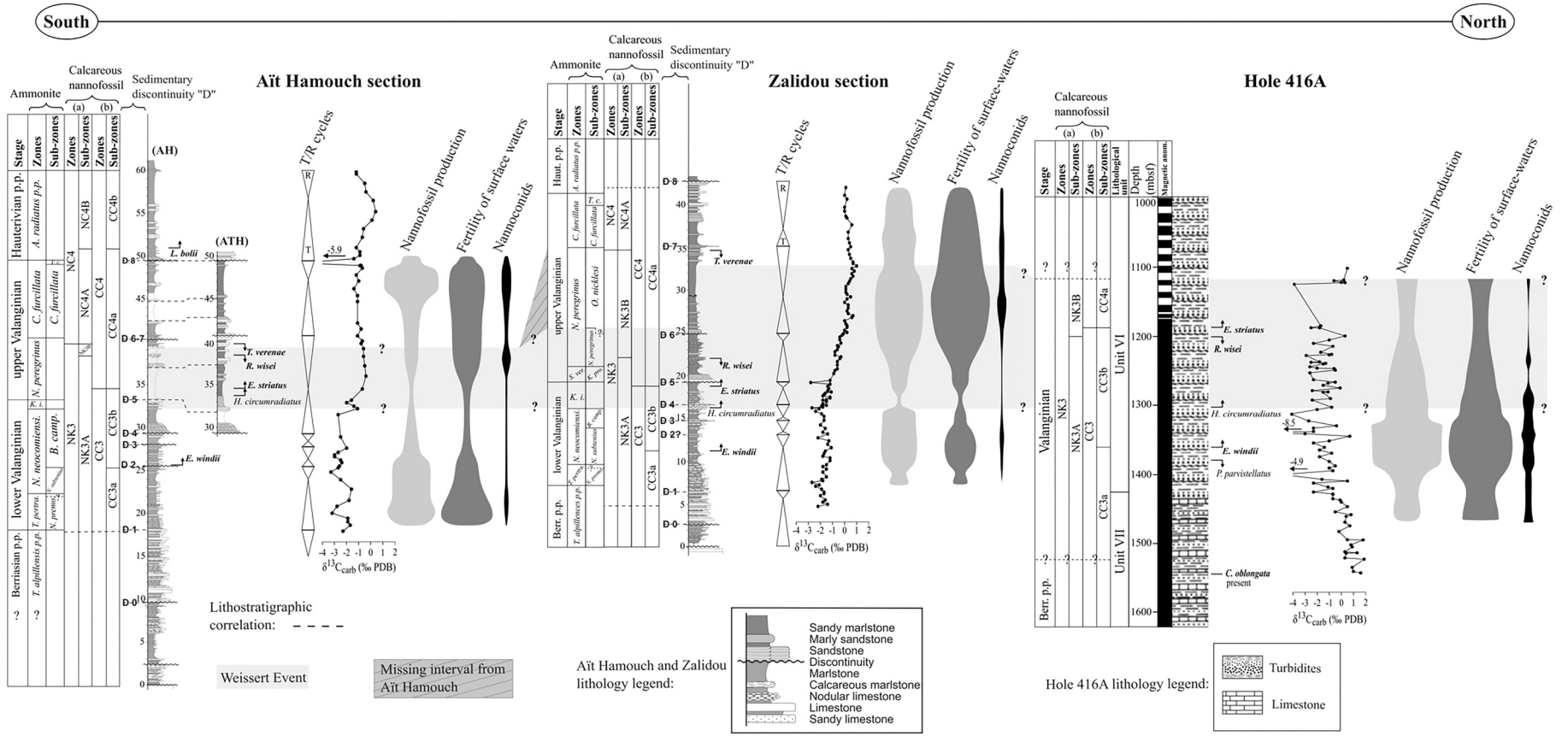

Fig. 10. Synthesis of the paleoceanographic conditions on the central Moroccan margin. Gray shading refers to the Weissert Event interval, for more details see Section 5.5. Striped-correlation refers to a possible missing interval in Aït Hamouch (Section 5.5). Simplified schemes of nannofossil production, fertility, and nannoconids abundance are comparable between Zalidou and Aït Hamouch since they are based on the accumulation rate results. Whereas, those of Hole 416A are based on the absolute abundance results. Also added are the transgression (T) - regression (R) cycles (Sections 5.1 and 5.2).

the smooth increase in $\delta^{13}C_{carb}$ within the CI positive shift is suspected to be missing from Aït Hamouch. This phase is observed during the *O. nicklesi* StSz in Zalidou (Fig. 10). Thereby, considering both the biostratigraphy of ammonites and calcareous nannofossils along with the chemostratigraphy from carbon-isotope analysis, it is highly possible that part of the late Valanginian could be missing from Aït Hamouch. Furthermore, the paleoceanographic reconstruction from calcareous nannofossils at Zalidou showed a collapse in nannofossil production just after the onset of the identified Weissert Event interval (*K. inostranzewi* StZ; Fig. 10). The collapse was followed by an increase in both nannofossil production and surface-water fertility, and then by slightly decreasing nannofossil production and fertility during the rest of the Weissert Event interval. Using all the above-mentioned information, the Weissert Event interval at Aït Hamouch is cautiously identified from 32.2 to 39.2 m (Fig. 10). This identified Weissert Event interval starts just before the nannofossil production collapse, and terminates when both nannofossil production and surface-water fertility recover and prior to the LO of *T. verenae*. The LO of *T. verenae* demonstrates that it is a reliable event.

At Hole 416A, the measured $\delta^{13}C_{carb}$ values do not show any positive shift (Fig. 6). Wortmann and Weissert (2000) measured $\delta^{13}C_{org}$ in samples from Hole 416A and identified a $\delta^{13}C_{org}$ positive excursion from −1420 to −1300 mbsf, which is not recognized in this study (Fig. 6). In both onshore sections, the base of the Weissert Event is roughly near to the FO of *H. circumradiatus*, although we acknowledge its occurrence is very sporadic. Therefore, we tentatively consider the interval corresponding to the Weissert Event from −1303 to −1122 mbsf in Hole 416A (Fig. 10). Its base is after the onset of the decline in nannofossil production and surface-water fertility, similar to the observation from the onshore sections. The explanation for the absence of a CI positive shift at Hole 416A is unclear. The supposed positive shift might have been diluted by the highly reworked material and terrigenous supply, or concealed by the graded turbidite cycles and/or by the high sedimentation rates known for this interval (Lancelot et al., 1980; Schlager, 1980). Indeed, the Valanginian sediments at Hole 416A are more than 400 m thick (Lancelot et al., 1980). Furthermore, the carbonate sediments in all studied successions, including Hole 416A, generally present a similar order of magnitude to the $\delta^{13}C_{carb}$ values (~ −1.0‰).

In the Essaouira-Agadir Basin (EAB), the calibration of the Weissert Event with calcareous nannofossils allows the assignment of the CI positive shift to the upper NK3A-upper NK3B subzones (upper CC3b to "middle" CC4a). The base of the Event is close to the FO of *H. circumradiatus*, whereas its end coincides roughly with the LO of *T. verenae* (Fig. 10). The Zalidou section is the most appropriate section to study the Weissert Event in the EAB. Although sedimentological discontinuities and related hiatuses are present, it is the most complete section and well dated by ammonite and nannofossil biostratigraphy (Fig. 10). The $\delta^{13}C_{carb}$ clearly shows a carbon-isotope positive shift similar to that observed elsewhere.

5.6. Basin-wide paleoceanographic reconstruction

In the EAB, a high calcareous nannofossil production and mesotrophic surface-water conditions occurred in the early Valanginian before the Weissert Event interval. This time-interval was also characterized by a low energy depositional environment and a mild oxygen-depletion (see Section 5.1), which could infer stratification of the water-column. However, some differences existed between the different settings due to their respective paleogeographic location (Fig. 9). The nannofossil production was higher at Aït Hamouch with respect to Zalidou in the early Valanginian (Fig. 10). Aït Hamouch was more distal from the shoreline with respect to Zalidou (see Section 5.2; Fig. 9). Consequently, the greater depth of deposition at Aït Hamouch and its location farther from the coastline allowed the development of a large and diverse nannofossil community in a thicker photic zone. Also, trophic levels in surface waters were higher at Aït Hamouch than at Zalidou (Fig. 10). Nutrient input in the EAB was generally maintained from both, clastic river input and oceanic upwelling (see Sections 5.1 and 5.2). During the early Valanginian, the northern part of the EAB (Zalidou section) was less influenced by clastic river influx with respect to the southern part (Aït Hamouch; see Fig. 9). Moreover, Aït Hamouch was potentially fed by nutrients from the nearby upwelling system observed in the Obbay section. Although, the highest nannofossil production was in Hole 416A, being offshore with the thickest photic zone (Fig. 6, and Figs. Supp. 2–3). Fertility levels decreased prior to the Weissert Event interval in the late early Valanginian in all successions (Fig. 10). Nonetheless, a high nannofossil production was maintained by the eurytopic *W. barnesiae/fossacincta*. The fertility decrease was probably related to a major sea level fall recorded on the central Moroccan margin, and culminated with the expression of the D4 and D5 sedimentary discontinuities (Figs. 3 and 10). The sea level fall first impacted the nannofossil community of the distal Aït Hamouch section with the possible ocean-ward migration of the upwelling system away from this site, which should have consequently reduced nutrient input. At the same time, storm deposits and coarse clastic input are recorded at Aït Hamouch (Section 5.1). Additionally, more turbid surface-water due to riverine-clastic input must have favored the proliferation of the eurytopic *W. barnesiae/fossacincta*. Afterwards, the entire nannofossil community collapsed at the onset of the Weissert Event and in its lower part, around the early-late Valanginian transition (Fig. 10). Offshore, in Hole 416A, the onset of the surface-water fertility decline (upper NK3A and CC3b subzones) and the later collapse of the nannofossil community (NK3B and CC3b-CC4a subzones) seem to have occurred slightly later than in the EAB (Fig. 10). We similarly relate these changes to the maximum drop of sea level expressed by the D4 and D5 discontinuities in the EAB. The collapse is observed later in the distal Hole 416A possibly due to the hiatuses related to emergences observed on the platform which are not recorded in a deep setting. The nannofossil production gradually recovered during the Weissert Event in the early late Valanginian and was associated with a rising sea-level (Section 4.1, Fig. 10). Higher riverine clastic input is recorded in the north (Zalidou) with respect to the south (Aït Hamouch; see Fig. 9). High input of clastics and associated nutrients could explain the early recovery at Zalidou in the nannofossil production and in the abundance of high fertility taxa. At Aït Hamouch, the recovery occurred later, and can be explained by the nutrient input that started arriving from the upwelling system. Maximal nannofossil production along with eutrophic surface-waters are recorded only at Zalidou during the upper part of the Weissert Event interval in the late Valanginian (upper *N. peregrinus* to upper *O. nicklesi* ammonite StSz, NK3B and lower CC4a subzones; Fig. 10). Eutrophic surface-waters occurred during maximal flooding and continuous continental influx (Section 5.1, Fig. 10). Lastly, a decrease in both the nannofossil production and surface-water fertility occurred after the Weissert Event interval in the rest of the late Valanginian (Fig. 10). Although, trophic levels were higher compared with the early Valanginian. An abrupt increase in the nannofossil production and surface water fertility is observed only at Aït Hamouch during the late Valanginian (*C. furcillata* StZ, NC4A and upper CC4a subzones) after the Weissert Event. At this time, the depositional environment in Aït Hamouch corresponded to an outer shelf (Fig. 9), possibly with a thick photic zone for the nannofossils to flourish. Whereas, the depositional environment in Zalidou corresponded to a clastic shelf with higher turbidity responsible for a reduced photic zone.

The nannoconids in the EAB and Hole 416A, mainly represented by *N. steinmannii* (narrow-canal form), generally show a distal-to-proximal gradient with highest abundances in Hole 416A followed by Aït Hamouch and Zalidou, successively. Also, the nannoconids were "thriving" during periods of relatively high fertility in surface-waters in all studied successions (Fig. 10). Initially, this is observed in the early Valanginian onshore (*N. premolicus* StSz to lowermost *N. subtenuis* StSz in Aït Hamouch and *N. subtenuis* LSz in Zalidou section, lower NK3A and CC3a subzones) and in the lower part of the Valanginian interval

offshore. Then, a nannoconid decline is recorded onshore in the early Valanginian (*N. neocomiensiformis* to lower *N. peregrinus* StZ, NK3A to lower NK3B subzones, CC3b to lower CC4a subzones), earlier in the southernmost section Aït Hamouch (Fig. 10). Offshore, in Hole 416A, the decline occurred slightly later in the uppermost NK3A to lower NK3B and upper CC3b to lower CC4a subzones. On the central Moroccan margin, this decline can be explained by the drop of sea-level that negatively impacted the entire nannofossil community. A fall of sea-level reduces the size of the photic zone (thickness and geographic extent), and can thus explain the observed decrease within the nannoconid population. DSDP Hole 416A was impacted later due to its distal setting and thicker photic zone. Afterwards, the nannoconids recovered in the late Valanginian (upper *N. peregrinus* StZ, NK3A-NK3B and lower CC4a subzones) during the Weissert Event interval. The nannoconids recovery occurred during periods of relatively high surface-water fertility in all studied successions (Fig. 10). These time-intervals were characterized by a high sea-level, which allowed the development of a thicker photic-zone and consequently various habitats to be occupied. Moreover, during the late early and late Valanginian, the occurrence of thin-bedded HCS restricted to shallow marine beds suggests the occurrence of storms of low intensity (Section 5.1). This could suggest the absence of stratification in the water-column.

Different positions within the photic zone were proposed for narrow- and wide-canal *Nannoconus* (Table 1). At Aït Hamouch, the proportion of narrow-canal forms (mainly *N. steinmannii*) within the nannoconid population reached its highest value during the sea-level fall interval and coincided with maximum clastic input (Fig. 5). Afterwards, although the clastic input was reduced, the proportion of narrow-canal forms within the nannoconid population decreased all along the succession. Then, as shown for Hole 416A, high abundance of *N. steinmannii* was not associated with a stratified water column but occurred during high clastic input (see Section 5.4.3). This implies a shallow nutricline. Our results confirm the assumption of Mattioli et al. (2014) suggesting that *N. steinmannii* inhabited de-stratified surface waters.

5.7. Integrating the central Moroccan margin in a global paleoceanographic reconstruction

In order to globally reconstruct the fertility in surface-waters during the Weissert Event, the paleoceanographic conditions (reconstructed from calcareous nannofossil data) of the central Moroccan margin are compared with those of other basins. All of the considered studies used the following taxa (small *Zeugrhabdotus* spp., *B. ellipticum*, *D. ignotus*, and *D. lehmanii*) as indicators of high surface-water fertility.

In the early Valanginian, high surface-water fertility was suggested in the western Atlantic in DSDP 535 (Gulf of Mexico; Kessels et al., 2006). In the western and northern Altantic (DSDP 534A/603B), Bornemann and Mutterlose (2008) suggested that surface-water productivity was already increasing from the Berriasian-Valanginian boundary prior to the Weissert Event. Whereas, in the Tethys (Vocontian Basin, SE France), generally oligotrophic conditions were recorded in the earliest Valanginian (lowermost NK3 Zone). These oligotrophic conditions were followed by more mesotrophic surface-waters prior to the Weissert Event in the early Valanginian (lower NK3 Zone; Duchamp-Alphonse et al., 2007). In the EAB, and in Hole 416A, the nannofossil production and surface-water fertility were relatively high in the early Valanginian (*N. premolicus* StSz to *N. subtenuis* LSz, lower NK3 and lower CC3 subzones).

At the early-late Valanginian transition and/or during the incipient Weissert Event, increasing surface-water fertility was observed in several basins. In the Pacific (Site 1149B) and Tethys oceans (Lombardian Basin, northern Italy), higher fertility and primary productivity was demonstrated in the upper NK3 Zone to the NC4A Subzone (Erba et al., 2004; Erba and Tremolada, 2004). In the Vocontian Basin (SE France), increasing calcareous nannofossil fluxes resulted from an increase in surface-water fertility during the Weissert Event, with highest values recorded within the lower NK3B calcareous nannofossil Subzone (upper *B. Campylotoxus* to lower *S. verrucosum* ammonite zones; Gréselle et al., 2011; Mattioli et al., 2014). In the western and northern Atlantic (DSDP 534A and 603B), a further increase in surface-water primary productivity was observed during the NK3A Subzone and just prior to the carbon-isotope excursion (Bornemann and Mutterlose, 2008). Also, in the western Atlantic (DSDP 535), Kessels et al. (2006) interpreted higher surface-water fertility in the early late Valanginian. The central Moroccan margin complements these previous records, and similarly demonstrates increasing surface-water fertility and nannofossil production during the Weissert Event on the south Tethyan margin.

In the rest of the late Valanginian, during the end or after the Weissert Event, surface-water fertility was observed to globally decrease. In the western Atlantic (DSDP 535), trophic conditions decreased in the late Valanginian (Kessels et al., 2006). In the northern Tethys, a decrease in surface-water fertility was observed in the Lombardian Basin (northern Italy), during the NC4A Subzone when $\delta^{13}C_{carb}$ is decreasing (Erba and Tremolada, 2004). In the Vocontian Basin (SE France), a decrease in both nannofossil fluxes and fertility indicators was observed from the upper part of the Weissert Event (*N. peregrinus* Zone and upper NK3-lower NC4 subzones; Gréselle et al., 2011; Mattioli et al., 2014). Nonetheless, in the Lower Saxony Basin (northern Germany) surface-water fertility increased during the latest Valanginian (Möller et al., 2020). In the EAB, surface-water fertility and nannofossil production decreased at the top of the Weissert Event and after it, as seen in the most complete section of Zalidou. Although, the fertility remained higher than in the early Valanginian. In the Aït Hamouch section, an abrupt increase in surface-water fertility and nannofossil production related to a thick photic zone in an outer shelf setting was observed in the latest Valanginian (upper *C. furcillata* StZ, NC4A and upper CC4a subzones).

However, in other studied basins, marine surface-water fertility was stable during the Valanginian. In the northern-central Atlantic (DSDP 638, NW Spain), high surface-water fertility was observed throughout the Valanginian (Kessels et al., 2006). Further north in NE Greenland, which was a gateway between the Arctic Ocean and the northern Tethys, oligotrophic conditions were observed during the Valanginian (Pauly et al., 2012). In the eastern Tethys (south and east Carpathians), generally oligotrophic surface-waters were observed during the Berriasian-Valanginian interval, supported by stable nannofossil diversity and abundance (Melinte and Mutterlose, 2001). From the available data, the eastern and northernmost Tethys seem to have been characterized by unchanging paleoceanographic conditions during the Valanginian. This might have been linked to the physiographic characteristics of these basins and the associated atmospheric/oceanic circulation currents (see Price et al., 1995; Poulsen et al., 1998).

5.8. The nannoconid decline

The decrease in the nannoconid abundances is known as the “Nannoconid decline”, and is globally recorded to start before the Valanginian positive CIE and spans the Weissert Event (Channell et al., 1993; Bersezio et al., 2002; Erba and Tremolada, 2004; Pauly et al., 2012; Möller et al., 2015). In the western Atlantic, the decrease in the nannoconid abundances was observed from the NK3A to NC4A calcareous nannofossil subzones (DSDP 534A; Bornemann and Mutterlose, 2008). In the Vocontian Basin (SE France), a more complicated decline was observed, such that a first decline was recorded from the NK3A to lower NK3B calcareous nannofossil subzones. This was followed by a brief recovery, then by another decline from the upper NK3B Subzone to NC4 Zone (Barbarin et al., 2012). On the central Moroccan margin, the nannoconid decline similarly started prior to the CI positive-shift. It is generally recorded from the NK3A to lower NK3B subzones (CC3b to lower CC4a subzones). Several authors interpreted the decline to be due to enhanced continental-clastic influx and increased nannofossil primary productivity, and possibly under higher oceanic pCO_2 levels (Erba

and Tremolada, 2004; Barbarin et al., 2012; Duchamp-Alphonse et al., 2014). Increasing surface-water fertility induces the breakdown of the water-column stratification, and then the decrease in the nannoconid population. Various authors proposed that the distribution of narrow-canal versus intermediate and wide-canal *Nannoconus* is controlled by fluctuations in nutricline dynamics. In particular, a nutricline rise from the lower to the upper photic zone would lead to the decrease in the narrow-canal forms, these forms are interpreted as deep-dwellers under stratified waters (Erba, 1994, 2004; Duchamp-Alphonse et al., 2014). Since different habitats within the photic zone seem plausible for the big calcifying nannoconids, a deep-dwelling behavior for *N. steinmannii* can be challenged in this study (see Section 5.6) confirming the hypothesis of Mattioli et al. (2014). Furthermore, in the Vocontian Basin, high proportions of narrow-canal forms (mainly represented by *N. steinmannii*) correlate with high coccolith abundance (NK3B to lower NC4A calcareous nannofossil subzones; Angles section; Duchamp-Alphonse et al., 2007, 2014). In addition, the highest proportion of narrow-canal nannoconids are recorded within the Weissert Event in the composite section of Vergol/La Charce, when the values of nannofossil fluxes are the highest (Gréselle et al., 2011; Barbarin et al., 2012). On the central Moroccan margin, the nannoconid decline was probably caused by a sea-level fall that gave rise to higher turbidity in the surface-waters. Higher turbidity probably attenuated light penetration, reducing the photic zone and the development of the total nannoconid population. However, enhanced clastic input and associated nutrients led to a shallow nutricline that did not particularly impact *N. steinmannii*.

Moreover, the nannoconid recovery was observed to coincide with the high $\delta^{13}C_{carb}$ values in the Tethys (Vocontian Basin, France) and in the western and northern Atlantic (DSDP 534A and 603B; Erba and Tremolada, 2004; Bornemann and Mutterlose, 2008; Barbarin et al., 2012). This agrees with observations in the EAB, since nannoconids recover during the Weissert Event when the $\delta^{13}C_{carb}$ is high and under conditions of both, high nannofossil production and surface-water fertility. This suggests that nannoconids do not particularly disfavor such surface-water conditions.

6. Conclusions

The quantitative analyses of calcareous nannofossil assemblages from two onshore sections belonging to the Essaouira-Agadir Basin (SW Morocco) and one offshore succession (DSDP Hole 416A, east Atlantic Ocean) allowed to reconstruct the paleoceanographic conditions on a proximal-distal transect across the Valanginian Weissert Event. This reconstruction was done in a well-constrained ammonite (for onshore sections only) and nannofossil biostratigraphic and chemostratigraphic (carbon-isotopes) framework, along with a detailed sedimentological characterization.

The Weissert Event interval is identified in the onshore sections from the *Karakaschiceras inostranzewi* to upper *Neocomites peregrinus* Standard Zone (StZ) or from the upper NK3A to upper NK3B, and upper CC3b to "middle" CC4a calcareous nannofossil subzones. The Valanginian stage demonstrated variations in surface-water fertility and nannofossil production. A general paleoceanographic scheme is developed: (1) mesotrophic and favorable surface-water conditions for the nannofossil community prevailed before the Weissert Event time interval in the early Valanginian. (2) Surface-water fertility levels decreased prior to the Weissert Event interval, and a high nannofossil production was maintained by the eurytopic *Watznaueria barnesiae/fossacincta*. (3) A collapse of the nannofossil community during the onset of the Weissert Event interval at the early-late Valanginian transition was caused by a major sea-level fall. (4) A recovery followed in the early late Valanginian linked to the rising sea-level. (5) The recovery was followed by maximal nannofossil production associated with high surface-water fertility, recorded in the northern section during the upper part of the Weissert Event interval in the late Valanginian; or in the southern section after the Weissert Event interval in the latest Valanginian. Finally, (6) a decrease in both surface-water fertility and nannofossil production occurred after the Weissert Event interval, although they remained high compared with the early Valanginian. Moreover, the "nannoconid decline" occurred from the early Valanginian to the early late Valanginian. The nannoconid recovery occurred during conditions of high sea-level and high surface-water fertility.

Supplementary data to this article can be found online at https://doi.org/10.1016/j.marmicro.2022.102134.

Declaration of Competing Interest

The authors declare that they have no known competing financial interests or personal relationships that could have appeared to influence the work reported in this paper.

Acknowledgements

This work benefited from financial support by the Ministries of foreign affairs from France and Morocco (PHC project n° 031/STU/13), the French IRD, Campus France, and various grants from the ISTerre laboratory (Grenoble), the Laboratoire de Géologie de Lyon, the OSUG@2020 Labex, the CNRS SYSTER program, and IODP France soutien post-cruise. Additional grants were provided by the French government (bourse BGF), the doctoral school TUE of the Grenoble-Alpes University, and by the TRB team of ISTerre laboratory. We are grateful to the editor Ric Jordan and two anonymous reviewers for both corrections and comments which greatly improved the quality of an earlier version of the manuscript.

References

Aguado, R., Company, M., Castro, J.M., de Gea, G.A., Molina, J.M., Nieto, L.M., Ruiz-Ortiz, P.A., 2018. A new record of the Weissert episode from the Valanginian succession of Cehegín (Subbetic, SE Spain): Bio- and carbon isotope stratigraphy. Cretac. Res. 92, 122–137. https://doi.org/10.1016/j.cretres.2018.07.010.

Aguirre-Urreta, M.B., Price, G.D., Ruffell, A.H., Lazo, D.G., Kalin, R.M., Ogle, N., Rawson, P.F., 2008. Southern Hemisphere Early Cretaceous (Valanginian-Early Barremian) carbon and oxygen isotope curves from the Neuquén Basin, Argentina. Cretac. Res. 29, 87–99. https://doi.org/10.1016/j.cretres.2007.04.002.

Applegate, J.L., Bergen, J.A., 1988. Cretaceous calcareous nannofossil biostratigraphy of sediments recovered from the Galicia margin, ODP Leg 103. Proc. Ocean Drilling Program. Leg. 103, 293–348.

Aubry, M.-P., Bord, D., Beaufort, L., Kahn, A., Boyd, S., 2005. Trends in size changes in the coccolithophorids, calcareous nannoplankton, during the Mesozoic: A pilot study. Micropaleontology 51, 309–318. https://doi.org/10.2113/gsmicropal.51.4.309.

Barbarin, N., Bonin, A., Mattioli, E., Pucéat, E., Cappetta, H., Gréselle, B., Pittet, B., Vennin, E., Joachimski, M., 2012. Evidence for a complex Valanginian nannoconid decline in the Vocontian basin (South East France). Mar. Micropaleontol. 84–85, 37–53. https://doi.org/10.1016/j.marmicro.2011.11.005.

Bartolini, A., 2003. Cretaceous radiolarian biochronology and carbon isotope stratigraphy of ODP Site 1149 (northwestern Pacific, Nadezhda Basin). Proc. Ocean Drilling Program. Leg. 185, 1–17. https://doi.org/10.2973/odp.proc.sr.185.011.2003.

Beaufort, L., Barbarin, N., Gally, Y., 2014. Optical measurements to determine the thickness of calcite crystals and the mass of thin carbonate particles such as coccoliths. Nat. Protoc. https://doi.org/10.1038/nprot.2014.028.

Bersezio, R., Erba, E., Gorza, M., Riva, A., 2002. Berriasian-Aptian black shales of the Maiolica formation (Lombardian Basin, Southern Alps, Northern Italy): Local to global events. Palaeogeogr. Palaeoclimatol. Palaeoecol. 180, 253–275. https://doi.org/10.1016/S0031-0182(01)00416-3.

Bertotti, G., Gouiza, M., 2012. Post-rift vertical movements and horizontal deformations in the eastern margin of the Central Atlantic: Middle Jurassic to Early Cretaceous evolution of Morocco. Int. J. Earth Sci. (Geol. Rundsch.) 101, 2151–2165.

Bordiga, M., Bartol, M., Henderiks, J., 2015. Absolute nannofossil abundance estimates: Quantifying the pros and cons of different techniques. Rev. Micropaleontol. 58, 155–165. https://doi.org/10.1016/j.revmic.2015.05.002.

Bornemann, A., Mutterlose, J., 2006. Size analyses of the coccolith species *Biscutum constans* and *Watznaueria barnesiae* from the Late Albian "Niveau Breistroffer" (SE France): taxonomic and palaeoecological implications. Geobios 39, 599–615. https://doi.org/10.1016/j.geobios.2005.05.005.

Bornemann, A., Mutterlose, J., 2008. Calcareous nannofossil and $\delta^{13}C$ records from the Early Cretaceous of the Western Atlantic Ocean: Evidence for enhanced fertilization across the Berriasian-Valanginian transition. Palaios 23, 821–832. https://doi.org/10.2110/palo.2007.p07-076r.

Bornemann, A., Aschwer, U., Mutterlose, J., 2003. The impact of calcareous nannofossils on the pelagic carbonate accumulation across the Jurassic-Cretaceous boundary.

Palaeogeogr. Palaeoclimatol. Palaeoecol. 199, 187–228. https://doi.org/10.1016/S0031-0182(03)00507-8.
Bown, P.R., 2005. Early to mid-Cretaceous calcareous nannoplankton from the Northwest Pacific Ocean, Leg 198, Shatsky Rise. Proc. Ocean Drill. Program Leg. 198, 1–82. https://doi.org/10.2973/odp.proc.sr.198.103.2005.
Bown, P.R., Concheyro, A., 2004. Lower Cretaceous calcareous nannoplankton from the Neuquén Basin, Argentina. Mar. Micropaleontol. 52, 51–84. https://doi.org/10.1016/j.marmicro.2004.04.006.
Bown, P.R., Lees, J.A., Young, J.R., 2004. Calcareous nannoplankton evolution and diversity through time. In: Thierstein, H.R., Young, J.R. (Eds.), Coccolithophores: From Molecular Processes to Global Impact. Springer-Verlag, Berlin, Berlin, pp. 481–508. https://doi.org/10.1007/978-3-662-06278-4_18.
Bown, P.R., Young, J.R., 1997. Proposals for a revised classification system for calcareous nannoplankton. J. Nannoplankton Res. 19 (1), 15–47.
Bralower, T.J., 1987. Valanginian to Aptian calcareous nannofossil stratigraphy and correlation with the upper M-sequence magnetic anomalies. Mar. Micropaleontol. 11, 293–310. https://doi.org/10.1016/0377-8398(87)90003-X.
Bralower, T.J., Monechi, S., Thierstein, H.R., 1989. Calcareous nannofossil zonation of the Jurassic-Cretaceous boundary interval and correlation with the geomagnetic polarity timescale. Mar. Micropaleontol. 14, 153–235. https://doi.org/10.1016/0377-8398(89)90035-2.
Bralower, T.J., Leckie, R.M., Sliter, W.V., Thierstein, H.R., 1995. An integrated Cretaceous microfossil biostratigraphy. Geochronol. Time Scales Glob. Stratigr. Correl. https://doi.org/10.2110/pec.95.04.0065.
Brenneke, J.C., 1978. A comparison of the stable oxygen and carbon isotope composition of Early Cretaceous and Late Jurassic carbonates from DSDP Sites 105 and 367. Lancelot, Y., Siebold, E., et al. Initial Rep. Deep Sea Drill. Proj. 41, 937–955. https://doi.org/10.2973/dsdp.proc.41.135.1978.
Čepek, P., Gartner, S., 1980. Mesozoic calcareous nannofossils, Deep Sea Drilling Project Sites 415 and 416. Moroccan Basin 345–351. https://doi.org/10.2973/dsdp.proc.50.108.1980.
Channell, J.E.T., Erba, E., Lini, A., 1993. Magnetostratigraphic calibration of the Late Valanginian carbon isotope event in pelagic limestones from Northern Italy and Switzerland. Earth Planet. Sci. Lett. 118, 145–166. https://doi.org/10.1016/0012-821X(93)90165-6.
Charbonnier, G., Boulila, S., Gardin, S., Duchamp-Alphonse, S., Adatte, T., Spangenberg, J.E., Föllmi, K.B., Colin, C., Galbrun, B., 2013. Astronomical calibration of the Valanginian "Weissert" episode: the Orpierre marl-limestone succession (Vocontian Basin, southeastern France). Cretac. Res. 45, 25–42. https://doi.org/10.1016/j.cretres.2013.07.003.
Charbonnier, G., Duchamp-Alphonse, S., Deconinck, J.F., Adatte, T., Spangenberg, J.E., Colin, C., Föllmi, K.B., 2020. A global palaeoclimatic reconstruction for the Valanginian based on clay mineralogical and geochemical data. Earth-Sci. Rev. 202, 103092 https://doi.org/10.1016/j.earscirev.2020.103092.
Coccioni, R., Erba, E., Premoli-Silva, I., 1992. Barremian-Aptian calcareous plankton biostratigraphy from the Gorgo Cerbara section (Marche, Central Italy) and implications for plankton evolution. Cretac. Res. 13, 517–537. https://doi.org/10.1016/0195-6671(92)90015-I.
Company, M., Tavera, J.M., 2015. Lower Valanginian ammonite biostratigraphy in the Subbetic Domain (Betic Cordillera, southeastern Spain). Carnets Geol. 15 https://doi.org/10.4267/2042/56745.
Cotillon, P., Rio, M., 1984. Cyclic sedimentation in the Cretaceous of Deep Sea Drilling Project Sites 535 and 540 (Gulf of Mexico), 534 (Central Atlantic), and in the Vocontian Basin (France). Initial Rep. Deep Sea Drill. Proj. 77, 339–376. https://doi.org/10.2973/dsdp.proc.77.106.1984.
Crux, J.A., 1989. Biostratigraphy and palaeogeographical applications of Lower Cretaceous nannofossils from north-western Europe. In: Nannofossils and their applications; International nannofossil association conference, pp. 143–211.
Deres, F., Achéritéguy, J., 1980. Biostratigraphie des Nannoconides. Bull. Centres Rech. Explor. Prod. Elf-Aquitaine 4, 1–53.
Duchamp-Alphonse, S., Gardin, S., Fiet, N., Bartolini, A., Blamart, D., Pagel, M., 2007. Fertilization of the northwestern Tethys (Vocontian basin, SE France) during the Valanginian carbon isotope perturbation: Evidence from calcareous nannofossils and trace element data. Palaeogeogr. Palaeoclimatol. Palaeoecol. 243, 132–151. https://doi.org/10.1016/j.palaeo.2006.07.010.
Duchamp-Alphonse, S., Fiet, N., Adatte, T., Pagel, M., 2011. Climate and sea-level variations along the northwestern Tethyan margin during the Valanginian C-isotope excursion: mineralogical evidence from the Vocontian Basin (SE France). Palaeogeogr. Palaeoclimatol. Palaeoecol. 302, 243–254.
Duchamp-Alphonse, S., Gardin, S., Bartolini, A., 2014. Calcareous nannofossil response to the Weissert episode (Early Cretaceous): Implications for palaeoecological and palaeoceanographic reconstructions. Mar. Micropaleontol. 113, 65–78. https://doi.org/10.1016/j.marmicro.2014.10.002.
Dunham, R.J., 1962. Classification of carbonate rocks according to depositional texture. In: Ham, W.E. (Ed.), Classification of Carbonate Rocks, AAPG Mem., 1, pp. 108–121.
Eleson, J.W., Bralower, T.J., 2005. Evidence of changes in surface water temperature and productivity at the Cenomanian/Turonian Boundary. Micropaleontology. 51, 319–332. https://doi.org/10.2113/gsmicropal.51.4.319.
Ellouz, N., Patriat, M., Gaulier, J.M., Bouatmani, R., Sabounji, S., 2003. From rifting to Alpine inversion: Mesooic and Cenozoic subsidence history of some Moroccan basins. Sediment. Geol. 156, 185–212. https://doi.org/10.1016/S0037-0738(02)00288-9.
Erba, E., 1992. Middle Cretaceous calcareous nannofossils from the western Pacific (Leg 129): evidence for paleoequatorial crossings. Proc. Ocean Drill. Program Leg. 129, 189–201. https://doi.org/10.2973/odp.proc.sr.129.119.1992.
Erba, E., 1994. Nannofossils and superplumes: the early Aptian "nannoconid crisis". Paleoceanography 9, 483–501.
Erba, E., 2004. Calcareous nannofossils and Mesozoic oceanic anoxic events. Mar. Micropaleontol. 52, 85–106. https://doi.org/10.1016/j.marmicro.2004.04.007.
Erba, E., Quadrio, B., 1987. Biostratigrafia a Nannofossili calcarei Calpionellidi e Foraminiferi planctonici della Maiolica (Titoniano superiore—Aptiano) nelle Prealpi Bresciane (Italia Settentrionale). Riv. Ital. Paleontol. Stratigr. 93 (1), 3–108.
Erba, E., Tremolada, F., 2004. Nannofossil carbonate fluxes during the Early Cretaceous: Phytoplankton response to nutrification episodes, atmospheric CO_2, and anoxia. Paleoceanography 19, n/a-n/a. https://doi.org/10.1029/2003PA000884.
Erba, E., Castradori, D., Guasti, G., Ripepe, M., 1992. Calcareous nannofossils and Milankovitch cycles: the example of the Albian Gault Clay Formation (southern England). Palaeogeogr. Palaeoclimatol. Palaeoecol. 93, 47–69.
Erba, E., Bartolini, A., Larson, R.L., 2004. Valanginian Weissert oceanic anoxic event. Geology 32, 149–152. https://doi.org/10.1130/G20008.1.
Ettachfini, M., 2004. Les ammonites néocomiennes dans l'Atlas Atlantique (Maroc): Biostratigraphie, Paléontologie, Paléobiogéographie et Paléoécologie. Strata, Série 2, Vol. Mémoires 43, 1–225.
Fernández-Blanco, D., Gouiza, M., Charton, R., Kluge, C., Klaver, J., Brautigam, K., Bertotti, G., 2020. Anticline growth by shortening during crustal exhumation of the Moroccan Atlantic margin. J. Struct. Geol. 140, 104125.
Ferry, S., Masrour, N., Grosheny, D., 2007. Le Crétacé de la marge atlantique marocaine (région d'Agadir). Excursion du Groupe Français du Crétacé, Livret-guide, p. 70. https://hal.archives-ouvertes.fr/hal-00686791/document.
Föllmi, K.B., 1996. The phosphorus cycle, phosphogenesis and marine phosphate-rich deposits. Earth-Sci. Rev. 40, 55–124.
Föllmi, K.B., Godet, A., Bodin, S., Linder, P., 2006. Interactions between environmental change and shallow water carbonate buildup along the northern Tethyan margin and their impact on the Early Cretaceous carbon isotope record. Paleoceanography 21, 1–16. https://doi.org/10.1029/2006PA001313.
Frizon de Lamotte, D., Zizi, M., Missenard, Y., Hafid, M., El Azzouzi, M., Maury, R.C., Charrière, A., Taki, Z., Benammi, M., Michard, A., 2008. The Atlas system. Lect. Notes Earth Sci. 116, 133–202. https://doi.org/10.1007/978-3-540-77076-3_4.
Gale, A.S., Mutterlose, J., Batenburg, S., Gradstein, F.M., Agterberg, F.P., Ogg, J.G., Petrizzo, M.R., 2020. The Cretaceous Period. In: Geologic Time Scale 2020. Elsevier, pp. 1023–1086.
Geisen, M., Bollmann, J., Herrle, J.O., Mutterlose, J., Young, J.R., 1999. Calibration of the random settling technique for calculation of absolute abundances of calcareous nannoplankton. Micropaleontology 45, 437–442. https://doi.org/10.2307/1486125.
Giraud, F., Olivero, D., Baudin, F., 2003. Minor changes in surface-water fertility across the oceanic anoxic event 1d (latest Albian, SE France) evidenced by calcareous nannofossils. Int. J. Earth Sci. 92 (2), 267–284. https://doi.org/10.1007/s00531-003-0319-x.
Gómez-Dacal, A.R., Gómez-Peral, L.E., Spalletti, L.A., Sial, A.N., Siccardi, A., Poiré, D.G., 2018. First record of the Valanginian positive carbon isotope anomaly in the Mendoza shelf, Neuquén Basin, Argentina: Palaeoclimatic implications. Andean Geol. 45, 111–129. https://doi.org/10.5027/andgeov45n2-3059.
Gréselle, B., Pittet, B., Mattioli, E., Joachimski, M., Barbarin, N., Riquier, L., Reboulet, S., Pucéat, E., 2011. The Valanginian isotope event: A complex suite of palaeoenvironmental perturbations. Palaeogeogr. Palaeoclimatol. Palaeoecol. 306, 41–57. https://doi.org/10.1016/j.palaeo.2011.03.027.
Gröcke, D.R., Price, G.D., Robinson, S.A., Baraboshkin, E.Y., Mutterlose, J., Ruffell, A.H., 2005. The Upper Valanginian (Early Cretaceous) positive carbon-isotope event recorded in terrestrial plants. Earth Planet. Sci. Lett. 240, 495–509. https://doi.org/10.1016/j.epsl.2005.09.001.
Grün, W., Allemann, F., 1975. The Lower Cretaceous of Caravaca (Spain): Berriasian calcareous nannoplankton of the Miravetes Section (Subbetic Zone, Prov. of Murcia). Eclogae Geol. Helv. 68, 147–211. https://doi.org/10.5169/seals-164382.
Hammer, Ø., Harper, D.A.T., Ryan, P.D., 2001. PAST: Paleontological Statistics Software Package for Education and Data Analysis. Palaeontol. Electron. 4 (1), 9.
Haq, B.U., 2014. Cretaceous eustasy revisited. Glob. Planet. Chang. 113, 44–58. https://doi.org/10.1016/j.gloplacha.2013.12.007.
Hay, W.W., DeConto, R.M., Wold, C.N., Wilson, K.M., Voigt, S., Schulz, M., Wold, A.R., Dullo, W.C., Ronov, A.B., Balukhovsky, A.N., Söding, E., 1999. Alternative global Cretaceous paleogeography. Spec. Pap. Geol. Soc. Am. 332. https://doi.org/10.1130/0-8137-2332-9.1.
Hennig, S., Weissert, H., Bulot, L., 1999. C-isotope stratigraphy, a calibration tool between ammonite- and magnetostratigraphy: the Valanginian-Hauterivian transition. Geol. Carpath. 50, 91–96.
Herrle, J.O., 2002. Reconstructing nutricline dynamics of mid-Cretaceous oceans: Evidence from calcareous nannofossils from the Niveau Paquier black shale (SE France). Mar. Micropaleontol. 47, 307–321. https://doi.org/10.1016/S0377-8398(02)00133-0.
Herrle, J.O., Pross, J., Friedrich, O., Hemleben, C., 2003. Short-term environmental changes in the Cretaceous Tethyan Ocean: micropalaeontological evidence from the Early Albian Oceanic Anoxic Event 1b. Terra Nova 15 (1), 14–19. https://doi.org/10.1046/j.1365-3121.2003.00448.x.
Jaillard, E., Chihaoui, A., Latil, J.-L., Zghal, I., 2021. Sequences, discontinuities and water stratification in a low-energy ramp: the Early Albian sedimentation in central Tunisia. Int. J. Earth Sci. 110, 263–285.
Kender, S., Kaminski, M.A., 2017. Modern deep-water agglutinated foraminifera from IODP Expedition 323, Bering Sea: ecological and taxonomic implications. J. Micropalaeontol. 36, 195–218.
Kenjo, S., Reboulet, S., Mattioli, E., Ma'louleh, K., 2021. The Berriasian–Valanginian boundary in the Mediterranean Province of the Tethyan Realm: Ammonite and

calcareous nannofossil biostratigraphy of the Vergol section (Montbrun-les-Bains, SE France), candidate for the Valanginian GSSP. Cretac. Res. 121, 104738 https://doi.org/10.1016/j.cretres.2020.104738.

Kessels, K., Mutterlose, J., Michalzik, D., 2006. Early Cretaceous (Valanginian - Hauterivian) calcareous nannofossils and isotopes of the northern hemisphere: Proxies for the understanding of Cretaceous climate. Lethaia 39, 157–172. https://doi.org/10.1080/00241160600763925.

Kuhnt, W., Moullade, M., Kaminski, M.A., 1996. Ecological structuring and evolution of deep-sea agglutinated foraminifera – a review. Rev. Micropaleontol. 39, 271–281.

Kujau, A., Heimhofer, U., Ostertag-Henning, C., Gréselle, B., Mutterlose, J., 2012. No evidence for anoxia during the Valanginian carbon isotope event - an organic-geochemical study from the Vocontian Basin, SE France. Glob. Planet. Change 92, 92–104. https://doi.org/10.1016/j.gloplacha.2012.04.007.

Kujau, A., Heimhofer, U., Hochuli, P.A., Pauly, S., Morales, C., Adatte, T., Föllmi, K., Ploch, I., Mutterlose, J., 2013. Reconstructing Valanginian (Early Cretaceous) mid-latitude vegetation and climate dynamics based on spore-pollen assemblages. Rev. Palaeobot. Palynol. 197, 50–69. https://doi.org/10.1016/j.revpalbo.2013.05.003.

Lancelot, Y., Winterer, E.L., Bosellini, A., Boutefeu, G.A., Boyce, R.E., Cepek, P., Fritz, D., Galimov, E.M., Melguen, M., Price, I., Schlager, W., Sliter, W., Taguchi, K., Vincent, E., Westberg, J., 1980. Site 416, in the Moroccan Basin, Deep Sea Drilling Project Leg 50. Initial Rep. Deep Sea Drill. Proj. 50, 115–301. https://doi.org/10.2973/dsdp.proc.50.104.1980.

Lees, J.A., 2002. Calcareous nannofossil biogeography illustrates palaeoclimate change in the Late Cretaceous Indian Ocean. Cretac. Res. 23 (5), 537–634. https://doi.org/10.1006/cres.2003.1021.

Lees, J.A., Bown, P.R., Mattioli, E., 2005. Problems with proxies? Cautionary tales of calcareous nannofossil paleoenvironmental indicators. Micropaleontology 51, 333–343. https://doi.org/10.2113/gsmicropal.51.4.333.

Lini, A., Weissert, H., Erba, E., 1992. The Valanginian carbon isotope event: a first episode of greenhouse climate conditions during the Cretaceous. Terra Nova 4, 374–384. https://doi.org/10.1111/j.1365-3121.1992.tb00826.x.

Lozar, F., Tremolada, F., 2003. Calcareous nannofossil biostratigraphy of Cretaceous sediments recovered at ODP Site 1149 (Leg 185, Nadezhda Basin, western Pacific). Proc. Ocean Drill. Program Leg 185, 1–21. https://doi.org/10.2973/odp.proc.sr.185.010.2003.

Lupi, C., Bordiga, M., Sacchi, R., Galinetto, P., Beaufort, L., Cobianchi, M., 2016. Do sample preparation techniques affect the relative abundance of *Florisphaera profunda*? Mar. Micropaleontol. 127, 42–49. https://doi.org/10.1016/j.marmicro.2016.07.007.

Martinez, M., Deconinck, J.F., Pellenard, P., Riquier, L., Company, M., Reboulet, S., Moiroud, M., 2015. Astrochronology of the Valanginian-Hauterivian stages (Early Cretaceous): chronological relationships between the Paraná-Etendeka large igneous province and the Weissert and the Faraoni events. Glob. Planet. Chang. 131, 158–173. https://doi.org/10.1016/j.gloplacha.2015.06.001.

Mattioli, E., Pittet, B., Riquier, L., Grossi, V., 2014. The mid-Valanginian Weissert Event as recorded by calcareous nannoplankton in the Vocontian Basin. Palaeogeogr. Palaeoclimatol. Palaeoecol. 414, 472–485. https://doi.org/10.1016/j.palaeo.2014.09.030.

McArthur, J.M., Janssen, N.M.M., Reboulet, S., Leng, M.J., Thirlwall, M.F., van de Schootbrugge, B., 2007. Palaeotemperatures, polar ice-volume, and isotope stratigraphy (Mg/Ca, $\delta^{18}O$, $\delta^{13}C$, $^{87}Sr/^{86}Sr$): The Early Cretaceous (Berriasian, Valanginian, Hauterivian). Palaeogeogr. Palaeoclimatol. Palaeoecol. 248, 391–430. https://doi.org/10.1016/j.palaeo.2006.12.015.

Meissner, P., Mutterlose, J., Bodin, S., 2015. Latitudinal temperature trends in the northern hemisphere during the Early Cretaceous (Valanginian-Hauterivian). Palaeogeogr. Palaeoclimatol. Palaeoecol. 424, 17–39. https://doi.org/10.1016/j.palaeo.2015.02.003.

Melinte, M., Mutterlose, J., 2001. A Valanginian (Early Cretaceous) "boreal nannoplankton excursion" in sections from Romania. Mar. Micropaleontol. 43, 1–25. https://doi.org/10.1016/S0377-8398(01)00022-6.

Menini, A., Mattioli, E., Spangenberg, J.E., Pittet, B., Suan, G., 2019. New calcareous nannofossil and carbon isotope data for the Pliensbachian/Toarcian boundary (Early Jurassic) in the western Tethys and their paleoenvironmental implications. Newsl. Stratigr. 52, 173–196. https://doi.org/10.1127/nos/2018/0476.

Michel, J., Borgomano, J., Reijmer, J.J.G., 2018. Heterozoan carbonates: when, where and why? A synthesis on parameters controlling carbonate production and occurrences. Earth Sci. Rev. 182, 50–67.

Möller, C., Mutterlose, J., Alsen, P., 2015. Integrated stratigraphy of Lower Cretaceous sediments (Ryazanian–Hauterivian) from North-East Greenland. Palaeogeogr. Palaeoclimatol. Palaeoecol. 437, 85–97. https://doi.org/10.1016/j.palaeo.2015.07.014.

Möller, C., Bornemann, A., Mutterlose, J., 2020. Climate and paleoceanography controlled size variations of calcareous nannofossils during the Valanginian Weissert Event (Early Cretaceous). Mar. Micropaleontol. 157, 101875 https://doi.org/10.1016/j.marmicro.2020.101875.

Morales, C., Kujau, A., Heimhofer, U., Mutterlose, J., Spangenberg, J.E., Adatte, T., Ploch, I., Föllmi, K.B., 2015. Palaeoclimate and palaeoenvironmental changes through the onset of the Valanginian carbon-isotope excursion: Evidence from the Polish Basin. Palaeogeogr. Palaeoclimatol. Palaeoecol. 426, 183–198. https://doi.org/10.1016/j.palaeo.2015.03.013.

Müller, G., Gastner, M., 1971. The "Karbonat-Bombe", a simple device for the determination of carbonate content in sediment, soils, and other materials. Neues Jahrbuch für Mineralogie-Monatshefte 10, 466–469.

Mutterlose, J., 1991. Das Verteilungs- und Migrations-Muster des kalkigen Nannoplanktons in der Unterkreide Valangin-Apt NW-Deutschland. Palaeontographica. B 221, 27–152.

Mutterlose, J., 1992a. Lower Cretaceous nannofossil biostratigraphy off northwestern Australia (Leg 123). Proc. Ocean Drill. Program Leg 123, 343–368.

Mutterlose, J., 1992b. Migration and evolution patterns of floras and faunas in marine Early Cretaceous sediments of NW Europe. Palaeogeogr. Palaeoclimatol. Palaeoecol. 94, 261–282. https://doi.org/10.1016/0031-0182(92)90123-M.

Mutterlose, J., Kessels, K., 2000. Early Cretaceous calcareous nannofossils from high latitudes: Implications for palaeobiogeography and palaeoclimate. Palaeogeogr. Palaeoclimatol. Palaeoecol. 160, 347–372. https://doi.org/10.1016/S0031-0182(00)00082-1.

Mutterlose, J., Brumsack, H., Flögel, S., Hay, W., Klein, C., Langrock, U., Lipinski, M., Ricken, W., Söding, E., Stein, R., Swientek, O., 2003. The Greenland-Norwegian Seaway: A key area for understanding Late Jurassic to Early Cretaceous paleoenvironments. Paleoceanography 18 (1). https://doi.org/10.1029/2001PA000625.

Mutterlose, J., Bornemann, A., Herrle, J., 2005. Mesozoic calcareous nannofossils - state of the art. Paläontol. Z. 79, 113–133.

Mutterlose, J., Rawson, P.F., Reboulet, S., Baudin, F., Bulot, L., Emmanuel, L., Gardin, S., Martinez, M., Renard, M., 2020. The Global Boundary Stratotype Section and Point (GSSP) for the base of the Hauterivian Stage (Lower Cretaceous), La Charce, southeast France. Episodes J. Int. Geosci. https://doi.org/10.18814/epiiugs/2020/020072.

Noel, D., Breheret, J.G., Lambert, B., 1987. Enregistrement sedimentaire de floraisons phytoplanctoniques calcaires en milieu confine; synthese de donnees sur l'actuel et observations geologiques. Bulletin de la Société Géologique de France 3 (6), 1097–1106.

Nunn, E.V., Price, G.D., Gröcke, D.R., Baraboshkin, E.Y., Leng, M.J., Hart, M.B., 2010. The Valanginian positive carbon isotope event in Arctic Russia: Evidence from terrestrial and marine isotope records and implications for global carbon cycling. Cretac. Res. 31, 577–592. https://doi.org/10.1016/j.cretres.2010.07.007.

Ouajhain, B., Daoudi, L., Medina, F., Rocha, F., 2009. Contrôle paléogéographique de la sédimentation argileuse du Jurassique du bassin atlasique d'Essaouira (haut atlas occidental, Maroc). Comun. Geol. 96, 51–66.

Pauly, S., Mutterlose, J., Alsen, P., 2012. Early Cretaceous palaeoceanography of the Greenland-Norwegian Seaway evidenced by calcareous nannofossils. Mar. Micropaleontol. 90 (91), 72–85. https://doi.org/10.1016/j.marmicro.2012.04.004.

Perch-Nielsen, K., 1979. Calcareous nannofossils from the Cretaceous between the North Sea and the Mediterranean. Aspekte der Kreide Europas, IUGS Series A. 6, 223–272.

Perch-Nielsen, K., 1985. Mesozoic Calcareous nannofossils. In: Bolli, H.M., Saunders, J. B., Perch-Nielsen, K. (Eds.), Plankton Stratigraphy. Cambridge Universitry Press, Cambridge, pp. 329–426.

Peybernes, C., Giraud, F., Jaillard, E., Robert, E., Masrour, M., Aoutem, M., Içame, N., 2013. Stratigraphic framework and calcareous nannofossil productivity of the Essaouira-Agadir Basin (Morocco) during the Aptian-Early Albian: Comparison with the north-Tethyan margin. Cretac. Res. 39, 149–169. https://doi.org/10.1016/j.cretres.2012.02.017.

Pittet, B., Mattioli, E., 2002. The carbonate signal and calcareous nannofossil distribution in an Upper Jurassic section (Balingen-Tieringen, Late Oxfordian, southern Germany). Palaeogeogr. Palaeoclimatol. Palaeoecol. 179, 71–96. https://doi.org/10.1016/S0031-0182(01)00409-6.

Pohl, A., Laugié, M., Borgomano, J., Michel, J., Lanteaume, C., Scotese, C.R., Frau, C., Poli, E., Donnadieu, Y., 2019. Quantifying the paleogeographic driver of Cretaceous carbonate platform development using paleoecological niche modeling. Palaeogeogr. Palaeoclimatol. Palaeoecol. 514, 222–232. https://doi.org/10.1016/j.palaeo.2018.10.017.

Poulsen, C.J., Seidov, D., Barron, E.J., Peterson, W.H., 1998. The impact of paleogeographic evolution on the surface oceanic circulation and the marine environment within the mid-Cretaceous Tethys. Paleoceanography 13, 546–559. https://doi.org/10.1029/98PA01789.

Premoli Silvá, I., Erba, E., Emilia Tornaghi, M., 1989. Paleoenvironmental signals and changes in surface fertility in mid Cretaceous C_{org}-rich pelagic facies of the Fucoid Marls (Central Italy). Geobios 22, 225–236. https://doi.org/10.1016/S0016-6995(89)80059-2.

Price, G.D., Mutterlose, J., 2004. Isotopic signals from late Jurassic-early Cretaceous (Volgian-Valanginian) sub-Arctic belemnites, Yatria River, Western Siberia. J. Geol. Soc. Lond. 161, 959–968. https://doi.org/10.1144/0016-764903-169.

Price, G.D., Sellwood, B.W., Valdes, P.J., 1995. Sedimentological evaluation of general circulation model simulations for the "greenhouse" Earth: Cretaceous and Jurassic case studies. Sediment. Geol. 100, 159–180. https://doi.org/10.1016/0037-0738(95)00106-9.

Puhfal, P.K., Groat, L.A., 2017. Sedimentary and igneous phosphate deposits: formation and exploration. Econ. Geol. 112, 483–516.

Reboulet, S., 1996. L'évolution des ammonites du Valanginien-Hauterivien inférieur du bassin vocontien et de la plate-forme provençale (S-E de la France): relations avec la stratigraphie séquentielle et implications biostratigraphiques. Travaux et Documents des Laboratoires de Géologie de Lyon 137 (1), 3–371.

Reboulet, S., Mattioli, E., Pittet, B., Baudin, F., Olivero, D., Proux, O., 2003. Ammonoid and nannoplankton abundance in Valanginian (Early Cretaceous) limestone–marl successions from the Southeast France Basin: carbonate dilution or productivity? Palaeogeogr. Palaeoclimatol. Palaeoecol. 201, 113–139.

Reboulet, S., Szives, O., Aguirre-Urreta, B., Barragán, R., Company, M., Frau, C., Kakabadze, M.V., Klein, J., Moreno-Bedmar, J.A., Lukeneder, A., Pictet, A., Ploch, I., Raisossadat, S.N., Vašíček, Z., Baraboshkin, E.J., Mitta, V.V., 2018. Report on the 6th International meeting of the IUGS Lower Cretaceous Ammonite Working Group, the Kilian Group (Vienna, Austria, 20th August 2017). Cretac. Res. 91, 100–110. https://doi.org/10.1016/j.cretres.2018.05.008.

Reolid, M., Nagy, J., Rodríguez-Tovar, F.J., Olóriz, F., 2008. Foraminiferal assemblages as palaeoenvironmental bioindicators in Late Jurassic epicontinental Platforms: Relation with trophic conditions. Acta Palaeontol. Pol. 53, 705–722.

Roth, P.H., 1978. Cretaceous nannoplankton biostratigraphy and oceanography of the northwestern Atlantic Ocean. Initial Rep. Deep Sea Drill. Proj. 44, 731–759. https://doi.org/10.2973/dsdp.proc.44.134.1978.

Roth, P.H., 1981. Mid-Cretaceous calcareous nannoplankton from Central Pacific: implication for paleoceanography. Initial Rep. Deep Sea Drill. Proj. 75, 651–655.

Roth, P.H., 1983. Jurassic and Lower Cretaceous calcareous nannofossils in the western North Atlantic (Site 534): biostratigraphy, preservation, and some observations on biogeography and paleoceanography. Initial Rep. Deep Sea Drill. Proj. 76, 587–621. https://doi.org/10.2973/dsdp.proc.76.125.1983.

Roth, P.H., 1989. Ocean circulation and calcareous nannoplankton evolution during the Jurassic and Cretaceous. Palaeogeogr. Palaeoclimatol. Palaeoecol. 74 (1–2), 111–126. https://doi.org/10.1016/0031-0182(89)90022-9.

Roth, P.H., Bowdler, J.L., 1981. Middle Cretaceous calcareous nannoplankton biogeography and oceanography of the Atlantic Ocean. Soc. Econ. Paleontol. Miner. Spec. Publ. 32, 517–546.

Roth, P.H., Krumbach, K.R., 1986. Middle Cretaceous calcareous nannofossil biogeography and preservation in the Atlantic and Indian oceans: Implications for paleoceanography. Mar. Micropaleontol. 10, 235–266. https://doi.org/10.1016/0377-8398(86)90031-9.

Roth, P.H., Thierstein, H., 1972. Calcareous nannoplankton: Leg 14 of the Deep Sea Drilling Program. Initial Rep. Deep Sea Drill. Proj. 14, 421–486. https://doi.org/10.2973/dsdp.proc.14.114.1972.

Sahabi, M., Aslanian, D., Olivet, J.L., 2004. Un nouveau point de départ pour l'histoire de l'Atlantique central. Compt. Rendus Geosci. 336, 1041–1052. https://doi.org/10.1016/j.crte.2004.03.017.

Schlager, W., 1980. Mesozoic Calciturbidites in Deep Sea Drilling Project Hole 416A recognition of a Drowned Carbonate Platform. Initial Rep. Deep Sea Drill. Proj. 50, 733–749. https://doi.org/10.2973/dsdp.proc.50.138.1980.

Shmeit, M., 2021. Apports continentaux versus upwellings dans le déclenchement de l'événement océanique anoxique Weissert (~ 137 Ma): contraintes micropaléontologiques et isotopiques. Ph.D. Thesis. Univ. Grenoble Alpes, France, 304p.

Sissingh, W., 1977. Biostratigraphy of Cretaceous calcareous nannoplankton. Geol. Mijnb. 56, 37–65.

Sliter, W.V., 1980. Mesozoic foraminifers and deep-sea benthic environments from Deep Sea Drilling Project sites 415 and 416, eastern North Atlantic. Initial Rep. Deep Sea Drill. Proj. 50, 353–427. https://doi.org/10.2973/dsdp.proc.50.109.1980.

Sprovieri, M., Coccioni, R., Lirer, F., Pelosi, N., Lozar, F., 2006. Orbital tuning of a lower Cretaceous composite record (Maiolica Formation, central Italy). Paleoceanography 21 (4). https://doi.org/10.1029/2005PA001224.

Stets, J., Wurster, P., 1982. Atlas and Atlantic – structural relations. Geol. Northwest African Cont. Margin 69–85. https://doi.org/10.1007/978-3-642-68409-8_5.

Street, C., Bown, P.R., 2000. Palaeobiogeography of Early Cretaceous (Berriasian-Barremian) calcareous nannoplankton. Mar. Micropaleontol. 39, 265–291. https://doi.org/10.1016/S0377-8398(00)00024-4.

Suchéras-Marx, B., Escarguel, G., Ferreira, J., Hammer, Ø., 2019. Statistical confidence intervals for relative abundances and abundance-based ratios: Simple practical solutions for an old overlooked question. Mar. Micropaleontol. 151, 101751 https://doi.org/10.1016/j.marmicro.2019.101751.

Tari, G., Jabour, H., 2013. Salt tectonics along the Atlantic margin of Morocco. Geol. Soc. Lond., Spec. Publ. 369, 337–353.

Thierstein, H.R., 1980. Selective dissolution of Late Cretaceous and Earliest Tertiary calcareous nannofossils: experimental evidence. Cretac. Res. 1 (2), 165–176. https://doi.org/10.1016/0195-6671(80)90023-3.

Trabucho Alexandre, J., Van Gilst, R.I., Rodríguez-López, J.P., De Boer, P.L., 2011. The sedimentary expression of oceanic anoxic event 1b in the North Atlantic. Sedimentology 58 (5), 1217–1246. https://doi.org/10.1111/j.1365-3091.2010.01202.x.

Tremolada, F., Erba, E., Bralower, T.J., 2006. Late Barremian to early Aptian calcareous nannofossil paleoceanography and paleoecology from the Ocean Drilling Program Hole 641C (Galicia Margin). Cretac. Res. 27, 887–897. https://doi.org/10.1016/j.cretres.2006.04.007.

Watkins, D.K., 1989. Nannoplankton productivity fluctuations and rhythmically-bedded pelagic carbonates of the greenhorn limestone (upper Cretaceous). Palaeogeogr. Palaeoclimatol. Palaeoecol. 74, 75–86. https://doi.org/10.1016/0031-0182(89)90020-5.

Weissert, H., Erba, E., 2004. Volcanism, CO_2 and palaeoclimate: a Late Jurassic-Early Cretaceous carbon and oxygen isotope record. J. Geol. Soc. Lond. 161, 695–702. https://doi.org/10.1144/0016-764903-087.

Weissert, H., Lini, A., Föllmi, K.B., Kuhn, O., 1998. Correlation of Early Cretaceous carbon isotope stratigraphy and platform drowning events: A possible link? Palaeogeogr. Palaeoclimatol. Palaeoecol. 137, 189–203. https://doi.org/10.1016/S0031-0182(97)00109-0.

Williams, J.R., Bralower, T.J., 1995. Nannofossil assemblages, fine fraction stable isotopes, and the paleoceanography of the Valanginian-Barremian (Early Cretaceous) North Sea Basin. Paleoceanography 10, 815–839. https://doi.org/10.1029/95PA00977.

Wippich, M.G.E., 2001. Die tiefe Unter-Kreide (Berrias bis Unter-Hauterive) im südwestmarokkanischen Becken: Ammonitenfauna, Bio-und Sequenzstratigraphie. PhD thesis, Bochum University/Universitat Bochu, pp. 142.

Wippich, M.G.E., 2003. Valanginian (Early Cretaceous) ammonite faunas from the western High Atlas, Morocco, and the recognition of western Mediterranean "standard" zones. Cretac. Res. 24, 357–374. https://doi.org/10.1016/S0195-6671(03)00049-1.

Wortmann, U.G., Weissert, H., 2000. Tying platform drowning to perturbations of the global carbon cycle with a delta $\delta^{13}C_{Org}$-curve from the Valanginian of DSDP Site 416. Terra Nova 12, 289–294. https://doi.org/10.1046/j.1365-3121.2000.00312.x.

Young, J.R., Bown, P.R., Lees, J.A., 2017. Nannotax3 website. International Nannoplankton Association. Accessed 10 April 2022. URL: http://www.mikrotax.org/Nannotax3.